Article

Cell Host & Microbe

Inflammation-Modulated Metabolic Reprogramming Is Required for DUOX-Dependent Gut Immunity in *Drosophila*

Graphical Abstract

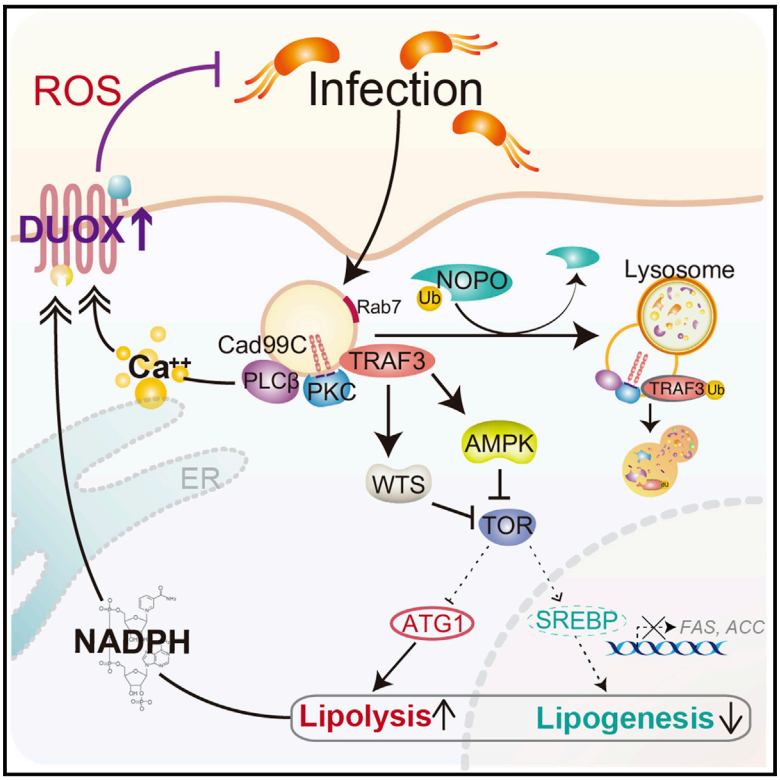

Highlights

- Enteric infection stimulates pro-catabolic signaling in the gut epithelia
- Infection induces metabolic reprogramming of gut epithelia toward lipid catabolism
- Gut metabolic reprogramming is required for DUOX activity and resistance to infection

Authors

Kyung-Ah Lee, Kyu-Chan Cho, Boram Kim, ..., Daehee Hwang, Jae-Hong Seol, Won-Jae Lee

Correspondence

lwj@snu.ac.kr

In Brief

DUOX, a member of the NADPH oxidase family, acts as the first line of host defense in the *Drosophila* intestine. Lee et al. show that pathogen infection stimulates pro-catabolic signaling that initiates metabolic reprogramming toward lipid catabolism, which is required for DUOX activation and host resistance to enteric infection.

Lee et al., 2018, Cell Host & Microbe *23*, 338–352
March 14, 2018
https://doi.org/10.1016/j.chom.2018.01.011

CellPress

CellPress

Cell Host & Microbe
Article

Inflammation-Modulated Metabolic Reprogramming Is Required for DUOX-Dependent Gut Immunity in *Drosophila*

Kyung-Ah Lee,[1,2,3,9] Kyu-Chan Cho,[1,9] Boram Kim,[1] In-Hwan Jang,[1,2,4] Kibum Nam,[1,2,4] Young Eun Kwon,[1,8] Myungjin Kim,[5] Do Young Hyeon,[6] Daehee Hwang,[7] Jae-Hong Seol,[1] and Won-Jae Lee[1,2,3,10,*]

[1]School of Biological Sciences, Seoul National University, Seoul 08826, South Korea
[2]National Creative Research Initiative Center for Hologenomics, Seoul National University, Seoul 08826, South Korea
[3]Institute of Molecular Biology and Genetics, Seoul National University, Seoul 151-742, South Korea
[4]Research Institute of Basic Sciences, IMCB, Seoul National University, Seoul 08826, South Korea
[5]Laboratory of Neurobiochemistry, Korea Brain Research Institute, Daegu 711-873, South Korea
[6]School of Interdisciplinary Bioscience and Bioengineering, POSTECH, Pohang 37673, South Korea
[7]Department of New Biology and Center for Plant Aging Research, Institute for Basic Science, DGIST, Daegu 711-873, South Korea
[8]Present address: Mogam Institute, Yongin 16924, South Korea
[9]These authors contributed equally
[10]Lead Contact
*Correspondence: lwj@snu.ac.kr
https://doi.org/10.1016/j.chom.2018.01.011

SUMMARY

DUOX, a member of the NADPH oxidase family, acts as the first line of defense against enteric pathogens by producing microbicidal reactive oxygen species. DUOX is activated upon enteric infection, but the mechanisms regulating DUOX activity remain incompletely understood. Using *Drosophila* genetic tools, we show that enteric infection results in "pro-catabolic" signaling that initiates metabolic reprogramming of enterocytes toward lipid catabolism, which ultimately governs DUOX homeostasis. Infection induces signaling cascades involving TRAF3 and kinases AMPK and WTS, which regulate TOR kinase to control the balance of lipogenesis versus lipolysis. Enhancing lipogenesis blocks DUOX activity, whereas stimulating lipolysis via ATG1-dependent lipophagy is required for DUOX activation. *Drosophila* with altered activity in TRAF3-AMPK/WTS-ATG1 pathway components exhibit abolished infection-induced lipolysis, reduced DUOX activation, and enhanced susceptibility to enteric infection. Thus, this work uncovers signaling cascades governing inflammation-induced metabolic reprogramming and provides insight into the pathophysiology of immune-metabolic interactions in the microbe-laden gut epithelia.

INTRODUCTION

Drosophila has been a successful model system for dissection of the molecular mechanisms of innate immunity (Buchon et al., 2014; Charroux and Royet, 2012; Lee and Brey, 2013; Lemaitre and Hoffmann, 2007; Mistry et al., 2016). Two nuclear factor κB (NF-κB) signaling pathways, Toll and immune deficiency (IMD), operate to produce NF-κB-dependent antimicrobial peptides in response to systemic infection (Lemaitre and Hoffmann, 2007). However, unlike internal germ-free organs involved in systemic immunity, mucosal epithelia of metazoans, mostly gut epithelia, are in constant contact with different microorganisms (Lee and Hase, 2014; McFall-Ngai et al., 2013; Shanahan, 2013). Most of these gut-associated microbes are considered as being commensal and/or symbiotic, whereas some of them may be pathogenic under certain circumstances (Hooper et al., 2012; Ryu et al., 2008). Despite the importance of gut-associated microbes, our understanding of this gut strategy of the microbe-controlling system, i.e., pathogen elimination versus commensal protection, remains incomplete. Genetic analyses of *Drosophila* gut immunity demonstrated that dual oxidase (DUOX), a member of nicotinamide adenine dinucleotide phosphate (NADPH) oxidase, acts as the first line of host defense against invading pathogens by producing microbicidal reactive oxygen species (ROS) (Ha et al., 2005, 2009b; Lee et al., 2013).

Due to the pivotal role of DUOX in gut immunity, the regulatory mechanism of the DUOX system has received considerable attention. Although the immunological roles of DUOX in mucosal epithelia seem to be conserved throughout the metazoans (e.g., *Caenorhabditis elegans*, insects, zebrafish, and rodents) (Flores et al., 2010; Grasberger et al., 2015; Lee et al., 2013; van der Hoeven et al., 2015; Yao et al., 2016), the regulatory mechanisms governing DUOX regulation have been studied extensively in *Drosophila*. Genetic studies in *Drosophila* showed that the DUOX-activity pathway is composed of phospholipase Cβ (PLCβ)-Ca^{2+} signaling to control DUOX enzymatic activity, whereas the DUOX-expression pathway is composed of the MEKK1-p38 MAPK pathway to control *DUOX* gene expression (Ha et al., 2009a, 2009b). It has been demonstrated that, unlike symbiotic bacteria, pathogens release the uracil molecule, and DUOX has been shown to be activated by the pathogen-derived uracil molecule (Lee et al., 2013). Recently, it has been shown that bacterial uracil induces Hedgehog (Hh) signaling activation, which acts as an upstream regulator of the DUOX-activity

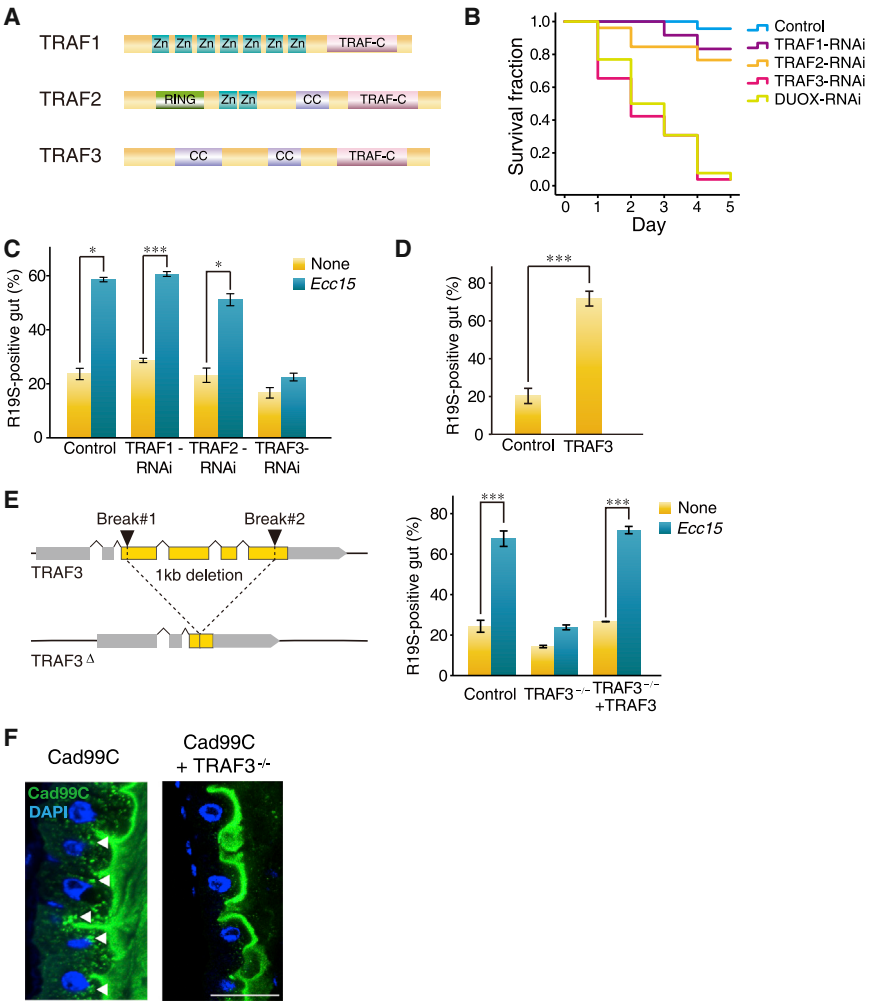

Figure 1. TRAF3 Is Required for DUOX Activation and Host Resistance against Enteric Infection

(A) Three *Drosophila* TRAF homologs. Zinc-binding motif (Zn), TRAF-C domain (TRAF-C), ring finger domain (RING), and coiled-coil domain (CC) are shown.

(B) Survival assay (n = 70–75 animals per genotype) following enteric infection with *Ecc15*. A log-rank analysis (Kaplan-Meier method) showed a significant difference in survival ($p < 0.001$) between control flies and *TRAF3-RNAi* flies.

(C) Infection-induced ROS generation. Adult flies (n = 30–50 guts per group) were orally infected with *Ecc15* for 1.5 hr.

(D) *TRAF3* overexpression is sufficient to induce spontaneous DUOX activation (n = 30–50 guts per group).

(E) The *TRAF3* genomic locus and mutant allele generated in this study (left panel). Open reading frame is indicated by yellow box. DUOX-dependent ROS generation is abolished in $TRAF3^{-/-}$ (right panel). Adult flies (n = 30–50 guts per group) were orally infected with *Ecc15* for 1.5 hr.

(F) Cad99C-positive endosome formation was abolished in the absence of *TRAF3*. Representative images from multiple experiments (n = 30–45 guts per group) are shown. Endosomes are indicated by arrowheads. Scale bar, 20 μm.

Data were analyzed using ANOVA followed by Tamhane's T2 post hoc test (C), Student's t test (D), or Tukey's post hoc test (E); values represent mean ± SEM (*$p < 0.05$, ***$p < 0.001$) of at least three independent experiments. Fly genotypes used in this study are shown in Table S4.

pathway (Lee et al., 2015). Hh pathway activation is required for uracil-induced *cadherin 99C* (*Cad99C*) expression in the apical region of enterocytes. Uracil-induced *Cad99C* expression further induces the formation of $Cad99C^{+}$ signaling endosomes to which PLCβ and protein kinase C (PKC) are recruited. Endosome formation was found to be necessary for PLCβ activity to increase intracellular calcium concentration for DUOX enzyme activation. Therefore, it is proposed that Hh-Cad99C pathway activation, $Cad99C^{+}$ endosome formation, PLCβ activation, PLCβ-dependent calcium mobilization, and DUOX activation are sequential events in the DUOX-activity pathway for the production of DUOX-dependent ROS (Lee et al., 2015). Flies carrying any functional mutation in Hh-Cad99C, PLCβ-Ca^{2+}, or MEKK1-p38 signaling pathways are highly susceptible to enteric infection due to impaired DUOX activity (Ha et al., 2009b; Lee et al., 2013, 2015). This highlights the importance of these signaling networks in DUOX-dependent gut immunity. The operation of such complex immune regulations may be energetically expensive. It has been recently suggested that infectious signals regulate cellular metabolic homeostasis to optimize the performance of the animal immune system (Zmora et al., 2017). However, the immune-metabolic interactions, especially at an organism level, are currently poorly understood.

Despite the extensive research conducted, the elucidation of the DUOX regulatory mechanism in *Drosophila* innate immunity remains incomplete. The objective of the present study was to obtain a more complete picture of the DUOX regulatory mechanism by taking advantage of the *Drosophila* genetic tools available. During our analyses, we found that bacterial infection acts as a pro-catabolic signal capable of initiating metabolic reprogramming of enterocytes toward lipid catabolism. Furthermore, we revealed that complex intracellular kinase cascades are involved in infection-modulated metabolic reprogramming. Finally, we showed that the infection-modulated metabolic reprogramming is necessary for cellular NADPH homeostasis, sustained DUOX activity, and host resistance against enteric infection, highlighting the importance of immune-metabolic interactions at an organism level.

RESULTS

TRAF3 Is Required for Host Resistance to Enteric Infection

The tumor necrosis factor receptor (TNFR)-associated factors (TRAFs) were originally identified as essential intracellular signaling molecules for the TNFR family throughout the metazoans (Ha et al., 2009c; Hacker et al., 2011). In *Drosophila* three TRAF genes, *TRAF1*, *TRAF2*, and *TRAF3* (also known as TRAF4,

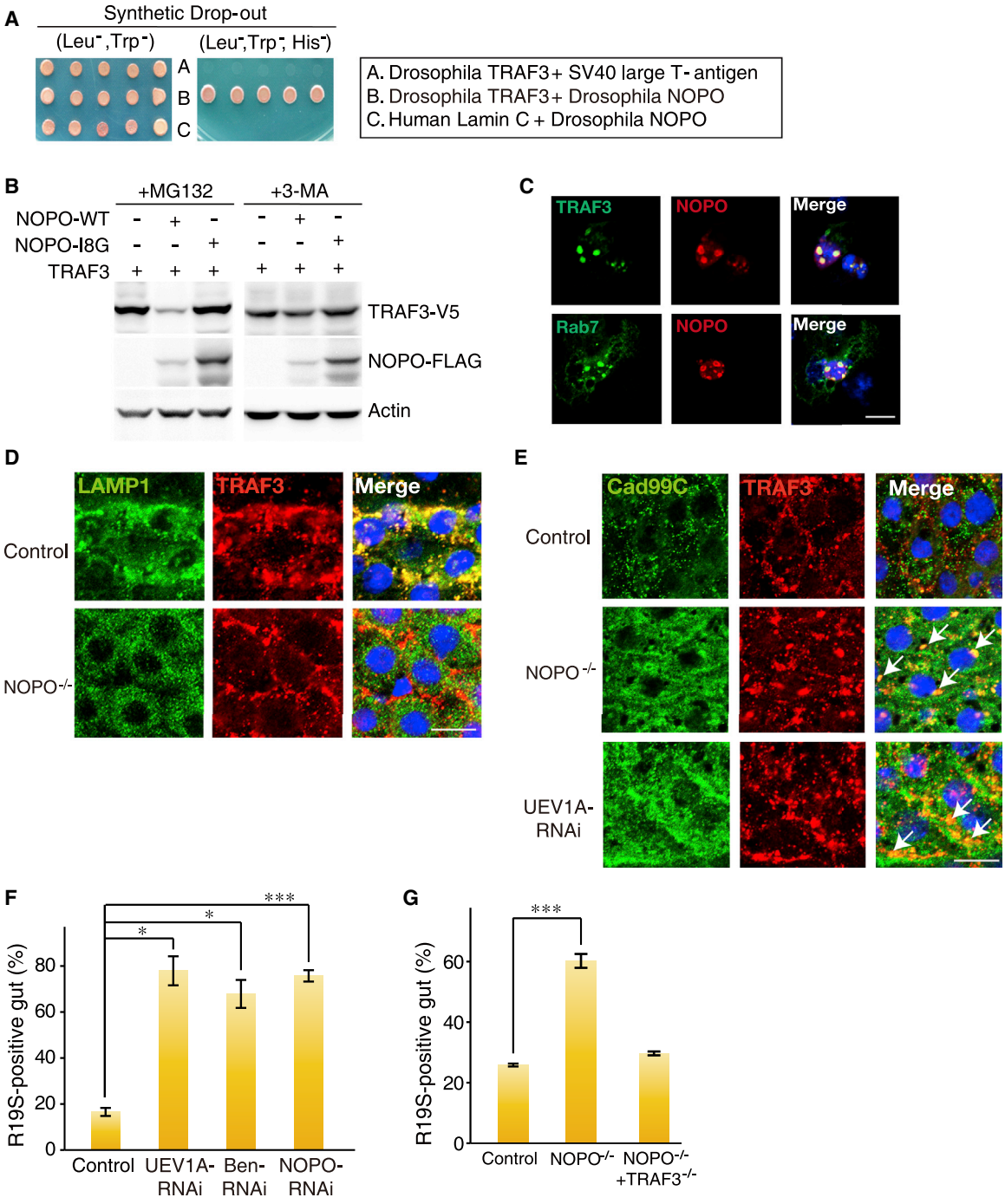

Figure 2. NOPO Is Involved in the Lysosomal Degradation of TRAF3 Protein and TRAF3$^+$ Endosomes

(A) Interaction between NOPO and TRAF3 in yeast two-hybrid assay. SV40 large T antigen and human lamin C were used as negative controls. Five independent transformants were spotted. Drop-out medium lacking Leu and Trp (Leu$^-$ Trp$^-$) was used to select co-transformants (left panel) and drop-out medium lacking Leu, Trp, and His (Leu$^-$ Trp$^-$ His$^-$) was used to visualize the interaction between NOPO and TRAF3 (right panel).

(B) NOPO induces TRAF3 degradation in a lysosome-dependent manner. Wild-type NOPO (NOPO-WT) or NOPO-I8G was co-transfected with TRAF3 into S2 cells in the presence of MG132 or 3-methyladenine.

(C) Co-localization of TRAF3 with NOPO on the Rab7$^+$ endosome. NOPO-I8G was used instead of wild-type NOPO to avoid TRAF3 degradation. Scale bar, 10 μm.

(D) TRAF3 was co-stained with LAMP1. Representative images from multiple experiments (n = 30–45 guts per group) are shown. Scale bar, 10 μm.

(E) Spontaneous TRAF3$^+$Cad99C$^+$ endosome formation (indicated by arrows) in the absence of UEV1A E2 enzyme or NOPO E3 enzyme. Representative images from multiple experiments (n = 30–45 guts per group) are shown. Scale bar, 10 μm.

(legend continued on next page)

TRAF6, and TRAF3, respectively, according to the sequence homologies with their mammalian counterparts), have been identified in the genome (Grech et al., 2000) (Figure 1A). It is well known that mammalian TRAFs are involved in innate immunity (Dempsey et al., 2003; Locksley et al., 2001). However, major immunological phenotypes (e.g., high host lethality following infection) of TRAF loss of function have not yet been reported in *Drosophila*. Therefore, we first examined the possible involvement of each TRAF in gut immunity. Assessment of the survival rate of enterocyte-specific knockdown RNAi flies for each TRAF following enteric infection showed that only *TRAF3-RNAi* flies were highly susceptible to enteric infection (Figure 1B). This finding indicated that *TRAF3* is required for gut innate immunity.

TRAF3 Is Required for Infection-Induced Cad99C^{+} Endosome Formation for DUOX Activation

It is well established that DUOX activity is required for gut innate immunity (Ha et al., 2005, 2009b; Lee et al., 2013). As *TRAF3-RNAi* flies are susceptible to enteric infection, similar to the case of the *DUOX-RNAi* animal (Figure 1B), we examined whether infection-induced DUOX activation is impaired in *TRAF3-RNAi* animals. When animals were subjected to enteric infection with a *Drosophila* natural pathogen, *Erwinia carotovora* supsp. *carotovora 15* (*Ecc15*), we found that enterocyte-specific *TRAF3-RNAi* animals failed to induce DUOX activation whereas the *TRAF1-RNAi* or *TRAF2-RNAi* animal showed normal DUOX activity (Figure 1C). Consistently, TRAF3 overexpression in the enterocytes is sufficient to induce spontaneous DUOX activation (Figure 1D). Furthermore, infection-induced DUOX activation was severely reduced in *TRAF3* null mutant animals generated by using CRISPR/Cas9 techniques (Figure 1E). Importantly, reduced DUOX activity found in *TRAF3* mutant animals could be restored by ectopic expression of *TRAF3* in enterocytes (Figure 1E), indicating that TRAF3 is required for infection-induced DUOX activity.

It has been shown that *Cad99C* overexpression is sufficient to induce spontaneous endosome formation and chronic DUOX activation under conventional (CV) conditions (i.e., in the presence of commensal and environmental bacteria) (Lee et al., 2015) (Figure 1F). Importantly, spontaneous Cad99C^{+} endosome formation (i.e., multiple foci in the enterocyte cytoplasm) observed in *Cad99C*-overexpressing CV flies was impaired under *TRAF3*$^{-/-}$ genetic background (Figure 1F). This result demonstrates that TRAF3 is required for Cad99C^{+} endosome formation for DUOX activation.

NOPO E3 Ligase Is Involved in the Lysosome-Dependent Degradation of TRAF3 *In Vitro*

Two public protein-protein interaction databases, BioGRID (https://thebiogrid.org/) and DroID (http://www.droidb.org/), as well as our yeast two-hybrid assay (Figure 2A), revealed that TRAF3 interacts with NOPO E3 ligase, previously known to be involved in the preservation of genomic integrity and apoptosis (Ma et al., 2012; Merkle et al., 2009; Wallace et al., 2014). E3 enzyme is a ubiquitin (Ub)-ligating enzyme working in concert with the Ub-activating (E1) and Ub-conjugating (E2) enzymes to accomplish Ub-dependent degradation of target proteins by either the proteasome-dependent or lysosome-dependent mechanism (Ciechanover, 2005). Therefore, we determined the role of these mechanisms on the NOPO-induced TRAF3 degradation by using *Drosophila* S2 cells. The results showed that NOPO overexpression was able to induce destabilization of TRAF3 protein levels (data not shown), and that the same phenomenon (i.e., NOPO-induced TRAF3 destabilization) was observed even in the presence of MG132, an inhibitor of proteasomal degradation (Figure 2B). However, NOPO-induced TRAF3 degradation could be abolished in the presence of 3-methyladenine, an inhibitor of lysosomal degradation (Figure 2B). These results indicate that NOPO negatively affects TRAF3 stability in a lysosome-dependent manner. Overexpression of a catalytically inactive NOPO mutant form (NOPO-I8G due to the replacement of Ile^{8} with Gly) had no effect on TRAF3 protein levels (Figure 2B), indicating that the E3 catalytic activity of NOPO is required for TRAF3 destabilization. We also observed a co-localization of TRAF3 and NOPO following overexpression in S2 cells (Figure 2C). Furthermore, these NOPO^{+} foci were stained by an endosome marker Rab7 (Figure 2C), indicating that TRAF3 and NOPO were co-localized on the endosomes. Collectively, these data indicate that TRAF3 is a target of NOPO E3 ligase and that NOPO is involved in the lysosome-dependent degradation of TRAF3 protein.

NOPO Is Involved in the Lysosomal Degradation of TRAF3^{+}Cad99C^{+} Endosomes

Given that NOPO degrades TRAF3 in a lysosome-dependent manner, it was hypothesized that NOPO is required for TRAF3^{+} endosome degradation via an endo-lysosomal degradation pathway. We found that TRAF3^{+} endosomes were co-localized with lysosome marker LAMP1 in control animals (Figure 2D). Importantly, LAMP1-co-localized TRAF3^{+} endo-lysosomes are absent in *NOPO*$^{-/-}$ animals (Figure 2D), indicating that the fusion between TRAF3^{+} endosomes and LAMP1^{+} lysosome is impaired in the absence of NOPO. Consistently, *NOPO*$^{-/-}$ flies show high basal levels of TRAF3^{+}Cad99C^{+} endosomes even under non-infectious conditions (Figure 2E).

NOPO E3 ligase is known to interact with E2 heterodimer, BEN, and UEV1A (Merkle et al., 2009). In agreement with this, we found that the knockdown of *UEV1A* is sufficient to induce high basal levels of TRAF3^{+}Cad99C^{+} endosome formation (Figure 2E), as in the case of *NOPO*$^{-/-}$ animals. Knockdown of any of *BEN-UEV1A-NOPO* results in spontaneous DUOX activation (Figure 2F) due to the accumulation of TRAF3^{+}Cad99C^{+} endosomes, indicating that BEN-UEV1A-NOPO acts as an E2-E3 complex responsible for the negative regulation of DUOX. Collectively, these results indicate that TRAF3 is required for both the endosome formation process (forming TRAF3^{+}Cad99C^{+} endosomes) and endosome degradation

(F) Spontaneous DUOX activation in knockdown of BEN-UEV1A-NOPO activity (n = 30–50 guts per genotype).
(G) High basal DUOX activity in *NOPO*$^{-/-}$ was abolished in the absence of *TRAF3* (n = 30–50 guts per genotype).
Data were analyzed using ANOVA followed by Tamhane's T2 post hoc test (F) or Tukey's post hoc test (G); values represent mean ± SEM (*$p < 0.05$, ***$p < 0.001$) of at least three independent experiments. Fly genotypes used in this study are shown in Table S4.

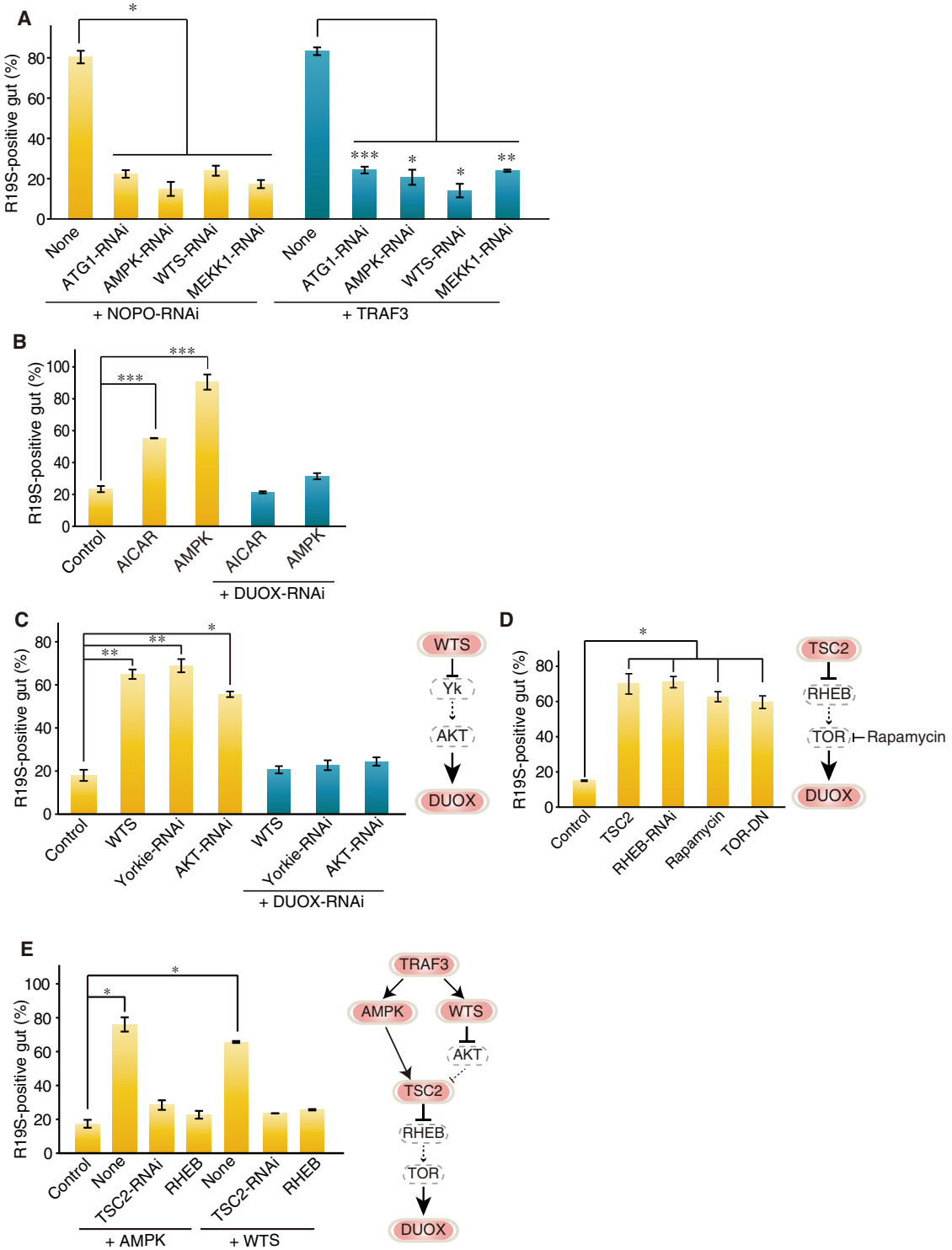

Figure 3. AMP-Activated Protein Kinase, WTS Kinase, ATG1 Kinase, and MEKK1 Are Identified as Downstream of TRAF3/NOPO for DUOX Activation

(A) Genetic screening. Knockdown of any of four kinases greatly suppressed the constitutive DUOX activation observed in *NOPO-RNAi*- or *TRAF3*-over-expressing animals.

(B) AMPK activation is sufficient to induce DUOX activation. Flies fed on 1 mM AICAR for 90 min.

(C) WTS-induced Yorkie-AKT inactivation is sufficient to induce DUOX activation. A model of the signaling pathway tested in this experiment is shown.

(legend continued on next page)

process (that occurs in an NOPO-dependent manner). Consistent with this idea, high DUOX activity observed in the *NOPO*$^{-/-}$ animals can be abolished under a *TRAF3*$^{-/-}$ genetic background (Figure 2G). These results indicate that TRAF3-dependent Cad99C^{+} endosome formation is an upstream event for NOPO-dependent Cad99C^{+} endosome degradation.

Genetic Screening Identified AMP-Activated Protein Kinase, WTS Kinase, ATG1 Kinase, and MEKK1 as Downstream of TRAF3/NOPO for DUOX Activation

We next investigated the NOPO downstream signaling pathway(s) to identify components involved in sustained DUOX activity in gut immunity. For this, suppressor screening was performed to identify signaling kinases capable of alleviating the *NOPO* mutant phenotype (i.e., constitutive DUOX activation). Using RNAi-based knockdown animals for the *Drosophila* primordial kinome of the 68 kinases (www.kinase.com) (Manning et al., 2002) (Table S1), we examined whether constitutive DUOX activation observed in *NOPO-RNAi* condition as well as *TRAF3* overexpression condition can be alleviated under an RNAi-based knockdown condition of each member of the 68 kinases. In this genetic screening, four kinases were identified (Figure 3A). These four kinases, acting as downstream regulators of TRAF3/NOPO, are the AMP-activated protein kinase (AMPK), Warts kinase (WTS, a core member of the Hippo pathway), autophagy-related 1 kinase (ATG1, a core member of the autophagy pathway), and MEKK1. MEKK1 was previously shown to be required for sustained DUOX activity by activating the *DUOX*-expression pathway (Ha et al., 2009b). Thus, we focused on the role of the three identified kinases (AMPK, WTS, and ATG1) on sustained DUOX activity.

AMPK Activation or WTS-Induced AKT Inactivation Is Sufficient to Induce DUOX Activation

It is well known that AMPK acts as a master metabolic regulator, playing an essential role in energy homeostasis (Shackelford and Shaw, 2009). When we induced spontaneous AMPK activation chemically (by ingestion of 5-aminoimidazole-4-carboxamide ribonucleotide [AICAR, an analog of AMP capable of activating AMPK]) or genetically (by overexpressing *AMPK*), we observed constitutive ROS generation in a DUOX-dependent manner (Figure 3B). Given that TRAF3-induced DUOX activation can be abolished under AMPK-RNAi conditions (Figure 3A), our results indicate that the activation of the TRAF3-AMPK pathway is sufficient for DUOX activation.

In the Hippo signaling pathway, WTS activation is known to inactivate Yorkie, a key transcriptional co-activator involved in the regulation of proliferation and growth-promoting genes (Yu and Guan, 2013). Similarly to AMPK, we found that overexpression of WTS or inactivation of Yorkie is sufficient to induce constitutive ROS generation in a DUOX-dependent manner (Figure 3C). Recently, it was shown that WTS activation and subsequent Yorkie inactivation lead to growth inhibition via AKT inhibition (Kwon et al., 2015). Consistently, AKT inhibition was also shown to be sufficient for the induction of spontaneous DUOX activation (Figure 3C). Epistatic analyses revealed that constitutive ROS generation found in Yorkie-RNAi flies was abolished under conditions of AKT activation (Figure S1), confirming that the inhibition of AKT acts as a downstream event of WTS-Yorkie for DUOX activation. These results indicate that the activation of the TRAF3-WTS pathway resulting in AKT inhibition is sufficient for DUOX activation.

AMPK Activation and WTS-Induced AKT Inactivation Induce DUOX Activation via TSC2 and RHEB-Mediated Inhibition of TOR

It is well known that the common downstream event of both AMPK activation and AKT inactivation is the activation of the tuberous sclerosis complex 2 (TSC2) (Saxton and Sabatini, 2017). TSC2 induces inactive form of Ras homolog enriched in brain (RHEB, a small guanosine triphosphatase [GTPase] protein) (Hardie, 2008) that inhibits the target of rapamycin (TOR) kinase activation (Saxton and Sabatini, 2017). When we reduced TOR activity by activating TSC2 (i.e., by using *TSC2*-overexpressing flies) or by inactivating RHEB (i.e., by using *RHEB-RNAi* flies), we observed spontaneous DUOX activation (Figure 3D). Consistently, spontaneous DUOX activation was also observed following chemical or genetic inhibition of TOR activity by ingestion of rapamycin or overexpression of the dominant-negative form of TOR kinase (TOR-DN) (Figure 3D). Importantly, AMPK and WTS pathway-induced activation of DUOX was abolished when we elevated TOR activity by inactivating TSC2 (i.e., by using *TSC2-RNAi* flies) or by activating RHEB (i.e., by using *RHEB*-overexpressing flies) (Figure 3E). Collectively, these results indicate that the inhibition of TOR kinase activity is sufficient to induce constitutive DUOX activation and that AMPK activation and WTS-induced AKT inactivation induce DUOX activation via TSC2-RHEB-mediated inhibition of TOR.

Infection Shapes the Lipid Metabolism of Gut Cells

TOR kinase is well known to act as a central regulator of cellular energy metabolism; TOR inhibition shifts energy homeostasis toward energy catabolism while downregulating energy anabolism (Laplante and Sabatini, 2012; Saxton and Sabatini, 2017). Based on this, we hypothesized that the enteric infection acts as a signal to induce metabolic reprogramming of the enterocytes. To test this hypothesis, we performed time-course mRNA-sequencing analysis of the *Drosophila* anterior midgut following enteric infection (Figure 4A and Table S2). Functional enrichment analyses revealed associations of these infection-modulated genes with different functional categories, most significantly (29.8%) "metabolism" (Figure 4B). Notably, lipid metabolism (27.0%)

(D) Inhibition of TOR kinase is sufficient to induce DUOX activation. Control flies fed on 5 μM rapamycin for 90 min. A model of the signaling pathway tested in this experiment is shown.

(E) AMPK and WTS pathway-induced DUOX activation was abolished by forced TOR activation. A model of the signaling pathway tested in this experiment is shown.

Data (n = 30–50 guts per genotype) were analyzed using ANOVA followed by Tamhane's T2 post hoc test (A and C–E) or Tukey's post hoc test (B); values represent mean ± SEM (*$p < 0.05$, **$p < 0.005$, ***$p < 0.001$) of at least three independent experiments. Fly genotypes used in this study are shown in Table S4.

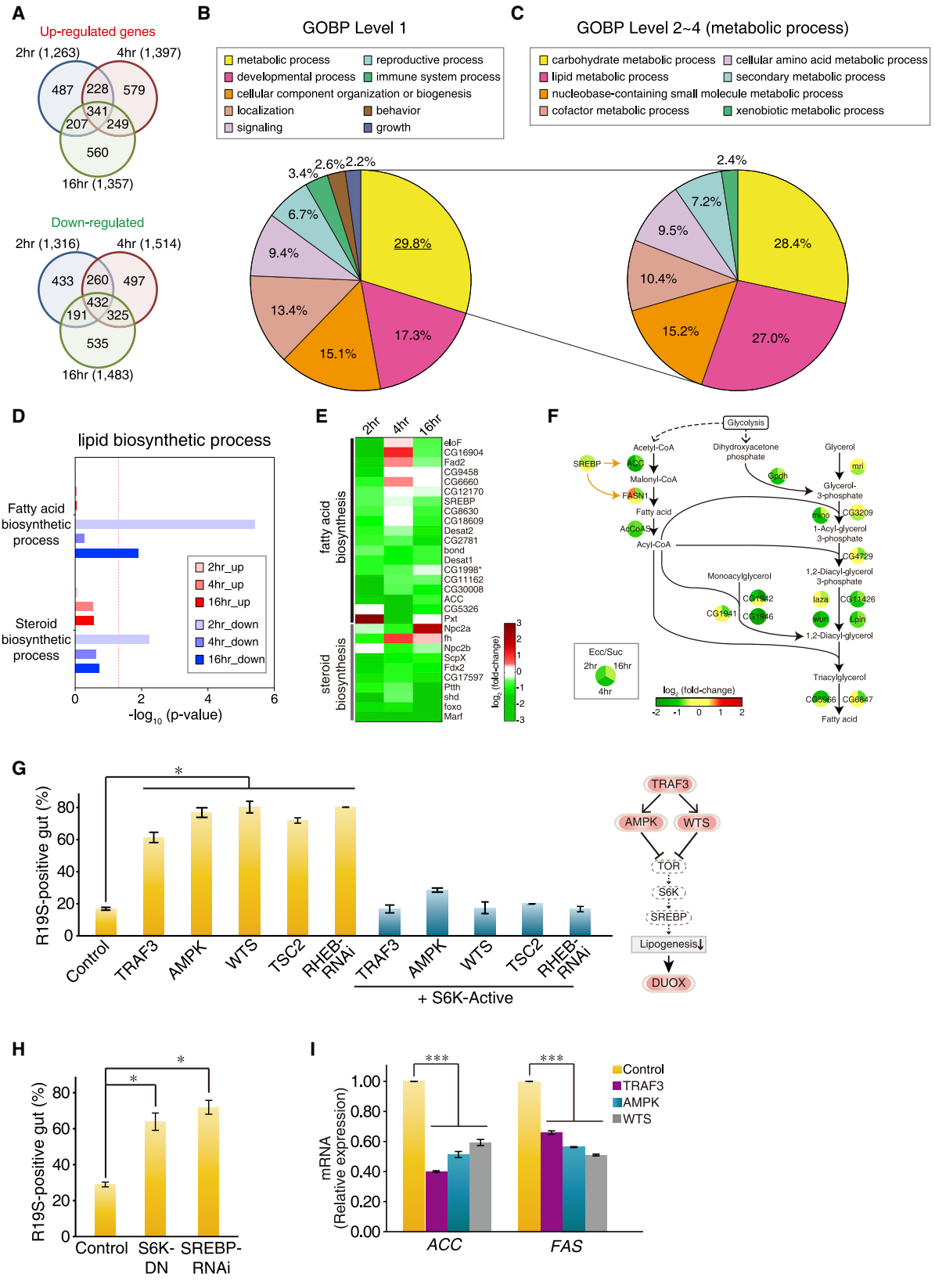

(legend on next page)

is one of mostly influenced processes by enteric infection among different metabolic processes (Figure 4C). We found that the expression of genes involved in the lipid anabolism pathways (i.e., fatty acid and steroid biosynthetic pathways) is greatly reduced upon enteric infection (Figures 4D–4F and S2). Taken together, our transcriptome analyses revealed that enteric infection shapes gut cell metabolism toward downregulation of lipid anabolism.

Repression of Lipogenesis by Inhibition of the TOR-S6K-SREBP Pathway Is Required for TRAF3-AMPK/WTS-Induced DUOX Activation

Activated TOR is known to induce ribosomal protein S6 kinase (S6K) activation and subsequent activation of sterol regulatory element-binding protein (SREBP, an S6K-dependent transcription factor). SREBP leads to the expression of major lipogenic genes such as *acetyl-CoA carboxylase* (*ACC*) and *fatty acid synthase* (*FAS*) for lipogenesis (Baker and Thummel, 2007; Laplante and Sabatini, 2009). Given that forced TOR activation can abolish AMPK- or WTS-induced DUOX activation (Figure 3E), we examined whether the ability of enhancing lipogenesis is sufficient to block DUOX activation. Flies overexpressing the active form of S6K (S6K-Active) or SREBP were used to enhance intestinal lipogenesis (Figure S3). Importantly, we found that enhancing lipogenesis is sufficient to block constitutive DUOX activation observed under conditions of TRAF3-AMPK/WTS pathway activation (overexpression of *TRAF3*, *AMPK*, or *WTS*) or TOR pathway inhibition (overexpression of *TSC2* or *RHEB-RNAi*) (Figure 4G). In contrast, flies carrying enterocyte-specific overexpression of the dominant-negative form of *S6K* (*S6K-DN*) or *SREBP-RNAi* (lipogenesis-reduced flies; see Figure S3) showed spontaneous DUOX activation (Figure 4H). As activation of the TRAF3-AMPK/WTS pathway is able to downregulate the TOR-S6K-SREBP pathway, as evidenced by the reduced expression levels of SREBP-dependent lipogenesis genes such as *ACC* and *FAS* (Figure 4I), we could conclude that repression of lipogenesis via inhibition of the TOR-S6K-SREBP pathway is an essential downstream event for TRAF3-AMPK/WTS pathway-induced activation of DUOX.

Enhancing Lipolysis by Activating the ATG1-Dependent Lipophagy Pathway Is Required for TRAF3-AMPK/WTS Pathway-Induced Activation of DUOX

TSC2/RHEB-mediated TOR inhibition not only downregulates lipogenesis but also upregulates lipolysis (Caron et al., 2015). Therefore, we investigated whether enhanced lipolysis is also involved in DUOX activation. Recently, autophagy-mediated lipolysis (lipophagy) showed that lipid droplets (LD, lipid-rich organelles mainly composed of triacylglyceride surrounded by a phospholipid monolayer) are sequestered by autophagosomes to give rise to LD-containing autophagosomes (i.e., lipophagosome formation) for lipolysis (Singh et al., 2009; Weidberg et al., 2009). When we quantified lipophagosome by counting the number of foci carrying both the autophagosome-marker ATG8 and lipid storage droplet 2 (LSD2, an LD marker), we found that ATG1 is required for lipophagosome formation (Figure 5A). Importantly, enhanced lipophagy and reduced cellular LD level were observed under TRAF3-AMPK/WTS pathway activation or TOR pathway inhibition conditions, when compared with control animals (Figures 5B and S4). These results indicate that ATG1-dependent lipophagy is activated by TRAF3-AMPK/WTS-induced inhibition of TOR. Consistent with these data, constitutive DUOX activation observed under the condition of enhanced lipophagy was abolished in the absence of ATG1 activity (Figure 5C). Furthermore, we found that the expression of genes involved in LD formation/expansion and its sequestration to autophagosome as well as its degradation in lysosome is elevated after enteric infection (Figures 5D and S5). Taken together, these results show that a metabolic shift toward lipid catabolism by activating the ATG1-dependent lipophagy pathway is required for TRAF3-AMPK/WTS pathway-induced activation of DUOX.

NADPH Homeostasis by Modulating Cellular Lipid Metabolism Is Required to Sustain DUOX Activity

As NOX/DUOX family enzymes use NADPH as a substrate, NADPH homeostasis is likely important for NADPH oxidase enzymatic activity (Leto and Geiszt, 2006). Given that lipogenesis consumes NADPH molecules whereas lipolysis generates NADPH molecules (Rui, 2014), both inhibition of lipid anabolism

Figure 4. Infection Shapes Lipid Metabolism for DUOX Activation

(A) Venn diagrams showing relationships among upregulated (upper panel) and downregulated (lower panel) genes at 2, 4, and 16 hr after enteric infection.

(B and C) Relative proportions of 4,965 differentially expressed genes in at least one time point after enteric infection according to their associated gene ontology biological processes (GOBPs). The GOBP terms at level 1 (B) and levels 2–4 (C) were used for general cellular processes and metabolic processes, respectively.

(D) Fatty acid and steroid biosynthetic processes enriched by the downregulated genes at each time point after enteric infection. The bars represent $-\log_{10}$ (p value) where p value from DAVID software is the significance of the processes being enriched by the up- or downregulated genes.

(E) Heatmap showing differential expression of the downregulated genes involved in fatty acid and steroid biosynthetic processes. The color bar shows the gradient of $\log_2$ fold changes of mRNA expression levels after enteric infection relative to control at each time point. The gene involved in both biosynthetic processes is indicated by an asterisk.

(F) Network model describing metabolic reactions by the downregulated genes involved in fatty acid synthesis. Black and orange arrows represent metabolic reactions and transcriptional regulation, respectively. The color bar represents the gradient of $\log_2$ fold changes of mRNA expression levels after enteric infection relative to control at each time point.

(G) Enhancing lipogenesis by S6K activation can abolish TRAF3-AMPK/WTS-TOR-mediated DUOX activation. Overexpression of *TSC2* or *RHEB-RNAi* was used to inhibit TOR activity. A model of the signaling pathway tested in this experiment is shown.

(H) Repression of lipogenesis via inhibition of the TOR-S6K-SREBP pathway is sufficient to induce DUOX activation.

(I) TRAF3-AMPK/WTS pathway is able to downregulate the SREBP-dependent lipogenesis genes. Real-time PCR analysis of *ACC* and *FAS*. Target gene expression in the control flies was taken arbitrarily as 1. Relative expression levels are expressed as the means ± SEM (***$p < 0.001$) of at least three independent experiments (n = 20 guts per experiment).

Data (n = 30–50 guts per genotype) were analyzed using ANOVA followed by Tamhane's T2 post hoc test (G and H); values represent mean ± SEM (*$p < 0.05$) of at least three independent experiments. Fly genotypes used in this study are shown in Table S4.

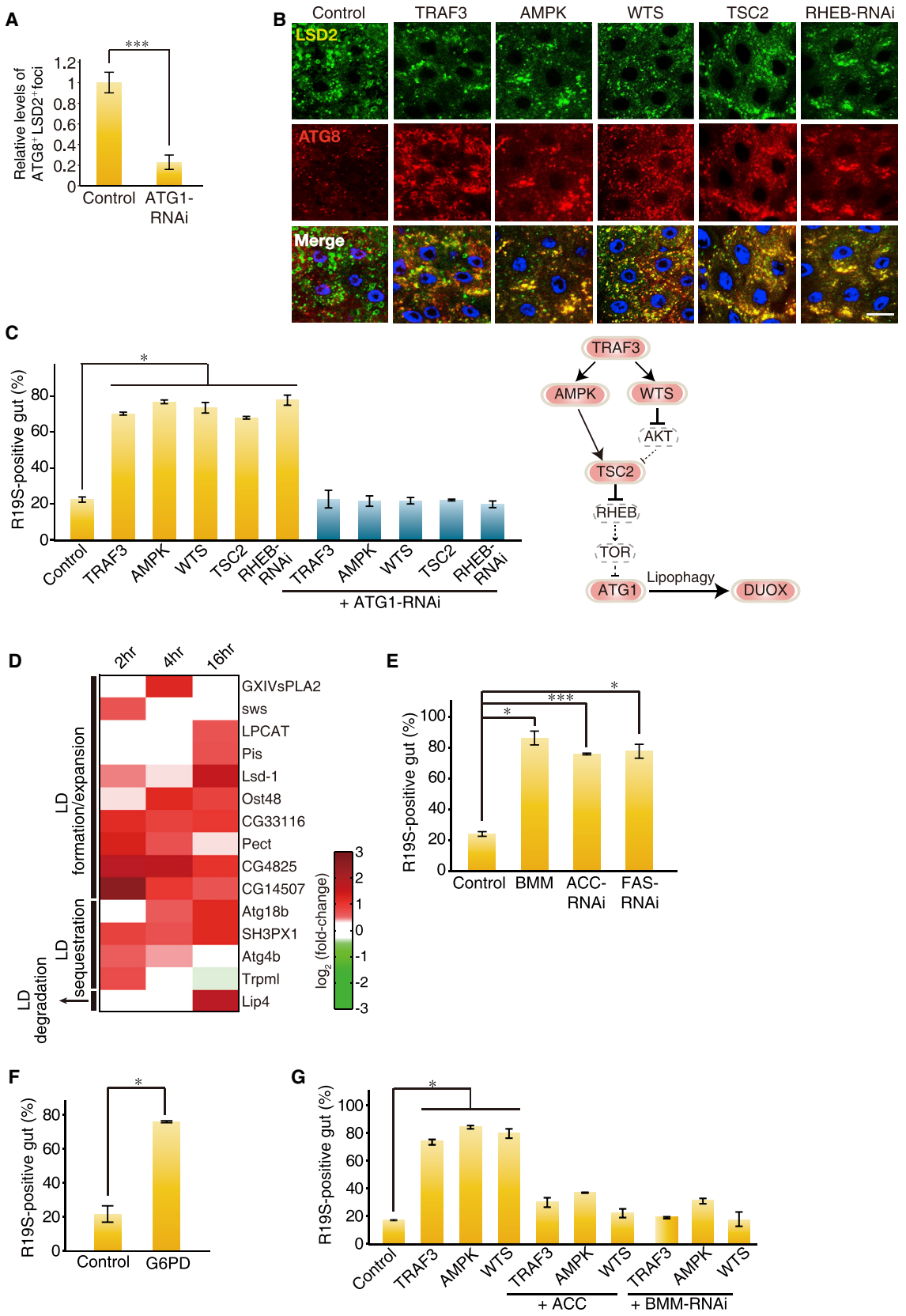

(legend on next page)

and enhancement of lipid catabolism may be required to maintain high NADPH levels for sustained DUOX activation during enteric infection. To test this hypothesis, we manipulated the levels of lipid metabolism in enterocytes by modulating key effector genes involved in lipid homeostasis. Strikingly, overexpression of a single gene involved in lipid catabolism such as *Brummer* (*BMM*, a *Drosophila* homolog of mammalian adipose TAG lipase) or downregulation of a single gene involved in lipid anabolism such as *ACC* or *FAS* is sufficient to induce constitutive DUOX activation (Figure 5E). Taken together, these results indicate that reducing NADPH consumption by downregulating lipogenic gene expression or enhancing NADPH generation by upregulating lipolytic gene expression is sufficient to induce spontaneous DUOX activation. Consistent with this notion, augmented NADPH levels in enterocytes by enhancing glycolysis (i.e., by overexpressing *glucose 6 phosphate dehydrogenase* [*G6PD*], a rate-limiting enzyme in the pentose phosphate pathway) is sufficient to induce constitutive DUOX activation (Figure 5F). Importantly, TRAF3-AMPK/WTS pathway-induced activation of DUOX can be abolished by overexpressing *ACC* or *BMM-RNAi* (Figure 5G), indicating that both repression of lipogenesis and enhancement of lipolysis are required for TRAF3-AMPK/WTS pathway-induced activation of DUOX. Collectively, these results indicate that NADPH homeostasis by regulating cellular lipid metabolism via modulation of the TRAF3-AMPK/WTS-ATG1 pathway activation is important to sustain DUOX activity.

A Metabolic Shift toward Lipid Catabolism via the TRAF3-AMPK/WTS-ATG1 Pathway Activation Is Required for Host Resistance to Enteric Infection

To evaluate the role of the TRAF3-AMPK/WTS-ATG1 signaling pathway in immune-metabolic interactions *in vivo*, we examined whether enteric infection is able to activate the TRAF3-AMPK/WTS-ATG1 signaling pathway, which is required for the metabolic shift to lipid catabolism. In the absence of infection, TRAF3 was primarily localized in the cytoplasm and membrane (Figure 6A). However, it was rapidly co-localized with Cad99C in the endosome upon enteric infection (Figure 6A). Importantly, infection-induced Cad99C^{+} endosome formation was completely abolished in the absence of *TRAF3* and restored by the reintroduction of *TRAF3* into the *TRAF3*$^{-/-}$ animals (Figure 6B). These results indicate that TRAF3 is required for infection-induced TRAF3^{+}Cad99C^{+} endosome formation. Furthermore, we also found that enteric infection can induce AMPK activation as evidenced by accumulation of the active form of AMPK in the membrane (Figure 6C), and WTS activation as evidenced by reduced activity of Yorkie target Ex-lacZ reporter (Figure 6D). The infection-induced AMPK and WTS activation were completely abolished in *TRAF3*$^{-/-}$ animals and restored by the reintroduction of *TRAF3* into the *TRAF3*$^{-/-}$ animals (Figures 6C and 6D). These results demonstrate that TRAF3 acts as an upstream regulator of both the AMPK and WTS pathway during enteric infection.

We next investigated whether enteric infection acts as a pro-catabolic signal capable of initiating metabolic shift toward lipolysis. We found that enteric infection rapidly induces lipophagy as evidenced by enhanced formation of ATG8^{+}LSD2^{+} lipophagosomes (Figure 6E). Previously, it has been shown that bacterial uracil induces Cad99C^{+} endosome formation via the Hh signaling pathway for DUOX activation (Lee et al., 2015). Therefore, we investigated whether uracil-induced Hh signaling is required to initiate lipid catabolism. The result showed that uracil ingestion leads to reduced cellular levels of LD in an Hh pathway-dependent manner (Figure S6). Furthermore, animals with constitutive Hh pathway activation such as *Costal-2* knockdown animals show low basal level of LD, indicating that Hh signaling acts as an upstream event of lipid catabolism (Figure S6). Importantly, infection-induced lipolysis of enterocytes was abolished in animals lacking activity of one of the TRAF3-AMPK/WTS-ATG1 pathway components (Figure 6E). These results demonstrate that the infection-induced lipid catabolism is occurring in a TRAF3-AMPK/WTS-ATG1 pathway-dependent manner. Consequently, animals lacking activity of one of the TRAF3-AMPK/WTS-ATG1 pathway components are unable to induce infection-induced DUOX activation (Figure 6F). These data confirm that infection-induced lipolysis is required for DUOX activation.

When we examined the survival rates of these pathway-mutant or -knockdown animals, we found high lethality following enteric infection (Figures 7A–7D and S7), highlighting the essential role of the TRAF3-AMPK/WTS-ATG1 pathway on host resistance to enteric infection. When the dysregulated metabolism observed in TRAF3-AMPK/WTS-ATG1 pathway-mutant

Figure 5. ATG1-Dependent Lipid Catabolism and NADPH Homeostasis Are Required for DUOX Activation

(A) Basal level of ATG8^{+}LSD2^{+} lipophagosome formation was abolished in *ATG1-RNAi* animals. RFP^{+}YFP^{+} foci were measured (n = 100 cells from 10 animals) using ImageJ (NIH). Number of RFP^{+}YFP^{+} foci in the control midguts was taken arbitrarily as 1. Relative levels of lipophagosome formation are expressed as the means ± SEM (***$p < 0.001$).

(B) ATG1-dependent lipophagy is activated by TRAF3-AMPK/WTS pathway activation or TOR inhibition. ATG8^{+}LSD2^{+} puncta formation was examined. Representative images from multiple experiments (n = 30–45 guts per genotype) are shown. Scale bar, 10 μm.

(C) Constitutive DUOX activation observed under TRAF3-AMPK/WTS pathway activation conditions or the TOR pathway inhibition conditions was abolished in the absence of ATG1 activity. A model of the signaling pathway tested in this experiment is shown. DUOX activity (n = 30–50 guts) for each genotype is shown.

(D) Heatmap showing differential expression of the upregulated genes involved in lipophagy. The color bar shows the gradient of $\log_2$ fold changes of mRNA expression levels after enteric infection relative to control at each time point.

(E) Upregulation of a single gene in lipid catabolism or downregulation of a single gene in lipid anabolism is sufficient to induce DUOX activation. DUOX activity (n = 30–50 guts) for each genotype is shown.

(F) Enhancement of glycolysis is sufficient to induce spontaneous DUOX activation. DUOX activity (n = 30–50 guts) for each genotype is shown.

(G) TRAF3-AMPK/WTS pathway-induced DUOX activation can be abolished by overexpressing *ACC* or *BMM-RNAi*. DUOX activity (n = 30–50 guts) for each genotype is shown.

Data were analyzed using ANOVA followed by Tamhane's T2 post hoc test (C, E, and G) or Student's t test (A and F); values represent mean ± SEM (*$p < 0.05$, ***$p < 0.001$) of at least three independent experiments. Fly genotypes used in this study are shown in Table S4.

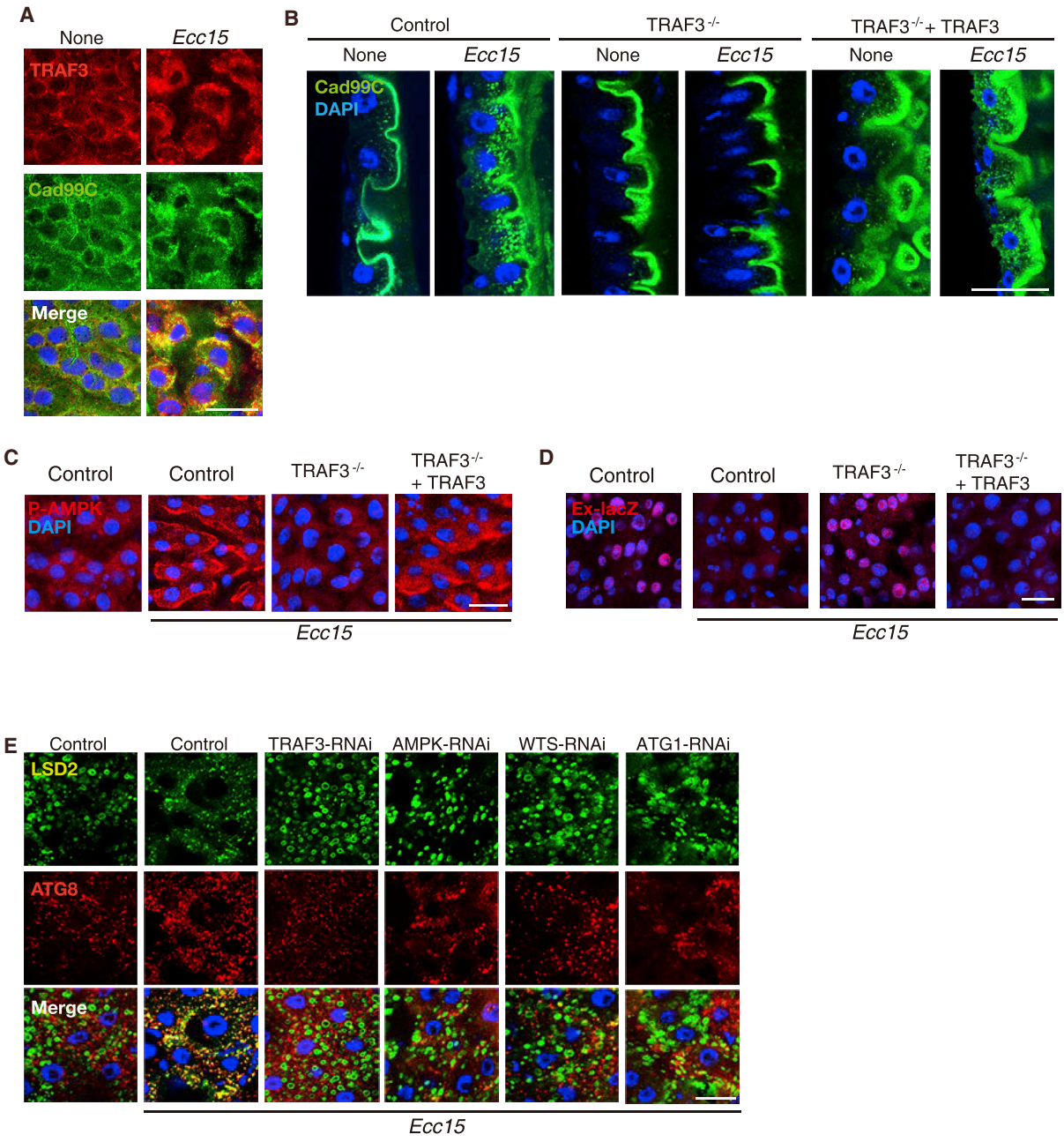

(legend on next page)

or -knockdown animals is corrected by either blocking lipogenesis (by *ACC-RNAi* overexpression), enhancing lipolysis (by *BMM* overexpression), or elevating NADPH-generating cellular glycolysis levels (by *G6PD* overexpression), the high infection-induced mortality rates of these flies were greatly rescued (Figures 7A–7D). These results demonstrate that the infection-induced metabolic shift for NADPH homeostasis via activation of the TRAF3-AMPK/WTS-ATG1 pathway is an essential event for sustained DUOX activity, which is required for host resistance to enteric infection.

DISCUSSION

Complex interactions among bacterial infection, host immunity, and metabolism are frequently observed in animals ranging from *Drosophila* to humans (Hotamisligil, 2006). For example, chronic systemic infection with pathogens such as *Mycobacterium* or *Listeria* is known to induce metabolic disorders such as wasting phenotype, exhibiting extensive loss of lipids and carbohydrates in both humans and *Drosophila* (Chambers et al., 2012; Dionne et al., 2006; Schwenk and Macallan, 2000). Similar host wasting was also observed in *Drosophila* in the case of enteric infection with *Vibrio cholerae* (Blow et al., 2005; Hang et al., 2014). However, it is unclear whether infection-induced metabolic wasting is a consequence of pathogen virulence or part of host immune response. Although immune-metabolic interactions are considered to be critical for host fitness during bacterial infection, the detailed signaling pathways by which pathogen infection regulates the host metabolism are not yet fully understood.

The present study was based on the well-characterized DUOX-dependent gut immunity in *Drosophila*. We found an unexpected link between the signaling pathways leading to DUOX-dependent intestinal immune activation and the pathways controlling lipid metabolism. Infection-induced DUOX-activating signaling exerted a pronounced effect on the metabolic requirement of enterocytes, leading to a metabolic shift from an energy-storing to an energy-consuming state. Our genetic screening identified four downstream kinases of TRAF3/NOPO (AMPK, WTS, ATG1, and MEKK1) capable of alleviating constitutive DUOX activation seen in *NOPO* knockdown or *TRAF3*-overexpressing conditions (Figure 3). AMPK, WTS, and ATG1 are representative metabolic signaling hubs known to be activated in response to nutritional and energy stress (Shackelford and Shaw, 2009; Singh and Cuervo, 2011; Yu and Guan, 2013). Our study revealed that these metabolic hubs are modulated by enteric infection (Figure 6), showing that activated TRAF3 signaling is found to be bifurcated into the WTS kinase and AMPK kinase pathways. What is the metabolic outcome of AMPK activation and WTS-induced AKT inhibition? It is well known that AMPK and AKT commonly phosphorylate TSC2 for activation and inactivation, respectively (Huang and Manning, 2008). AMPK induces the GTPase activity of TSC2 by phosphorylating its Ser^{1107} site, whereas AKT inhibits the GTPase activity of TSC2 by phosphorylating different sites of TSC2 (e.g., Ser^{924} and Thr^{1518}). Therefore, enteric infection may lead to an increase in Ser^{1107} phosphorylation and a decrease in Ser^{924}/Thr^{1518} phosphorylation, thereby resulting in a strong TSC2 activation. Therefore, enteric infection ultimately gave a signal for TOR inhibition via AMPK-WTS/AKT pathway-induced TSC2 activation. Infection-induced TOR inhibition leads to S6K inhibition for the suppression of NADPH-consuming lipogenesis while activating ATG1-dependent NADPH-yielding lipolysis. This infection-induced metabolic shift toward lipid catabolism is necessary to sustain DUOX activity by maintaining NADPH homeostasis, which is required for host resistance against enteric infection.

The relationship between inflammation and metabolism is poorly understood. The present study may provide an important conceptual framework for understanding the molecular crosstalk between gut immune activation and metabolic reprogramming. Previously, in a model of Toll/IMD-mediated systemic immunity, intracellular pathogens such as *Mycobacterium* or *Listeria* resulted in the wasting phenotype in *Drosophila* (Chambers et al., 2012; Dionne et al., 2006). In this case, inactivation of AKT activity produces pathological FOXO activation results in loss of anabolic activity, which is involved in the wasting phenotype (Dionne et al., 2006). Recently, activation of the bacterial-induced Toll/IMD pathway was shown to antagonize S6K activity for the modulation of MEF2 activity, resulting in loss of anabolism (Clark et al., 2013). Although inactivation of AKT and S6K is observed during systemic inflammation (Clark et al., 2013; Dionne et al., 2006), the relationship between S6K inhibition and AKT inhibition, and which signaling molecules act as upstream/downstream components of these kinases, are unclear. As inactivation of AKT and S6K in enterocytes is required for DUOX-dependent gut immunity (Figures 3 and 4), it is likely that infection-induced inactivation of AKT and S6K is commonly shared between Toll/IMD-based systemic immunity

Figure 6. Enteric Infection Induces Lipophagy-Dependent DUOX Activation via TRAF3-AMPK/WTS-ATG1 Pathway Activation

(A) Enteric infection induces $Cad99C^{+}TRAF3^{+}$ endosome formation. Flies carrying genomic fragment (7,486 bp) including ~5.2 kb of promoter, coding region, and ~0.8 kb 3′ UTR region of TRAF3 were used in the absence or presence of enteric infection (at 2 hr post infection). TRAF3 was V5 epitope-tagged in this genomic fragment.

(B) Enteric infection induces $Cad99C^{+}$ endosome formation (at 2 hr post infection) in a TRAF3-dependent manner. Adult male flies (5–6 days old) were used.

(C) Enteric infection induces AMPK activation in a TRAF3-dependent manner. Accumulation of active form of AMPK in the membrane was visualized by anti-phospho-AMPK antibody at 2 hr post infection. Adult male flies (5–6 days old) were used.

(D) Enteric infection induces WTS activation in a TRAF3-dependent manner. WTS activation was visualized by reduced activity of Ex-lacZ reporter at 2 hr post infection. Adult male flies (5–6 days old) were used.

(E) Enteric infection induces lipophagy in a TRAF3-AMPK/WTS-ATG1 pathway-dependent manner. $ATG8^{+}LSD2^{+}$ puncta formation was examined at 2 hr post infection.

(F) Enteric infection induces DUOX activation (at 1.5 hr post infection) in a TRAF3-AMPK/WTS-ATG1 pathway-dependent manner. Data (n = 30–50 guts per group) were analyzed using an ANOVA followed by Tamhane's T2 post hoc test; values represent mean ± SEM (*$p < 0.05$) of at least three independent experiments. In (A) to (E), representative images from multiple experiments (n = 30–45 guts per genotype) are shown. Scale bar, 20 μm. Fly genotypes used in this study are shown in Table S4.

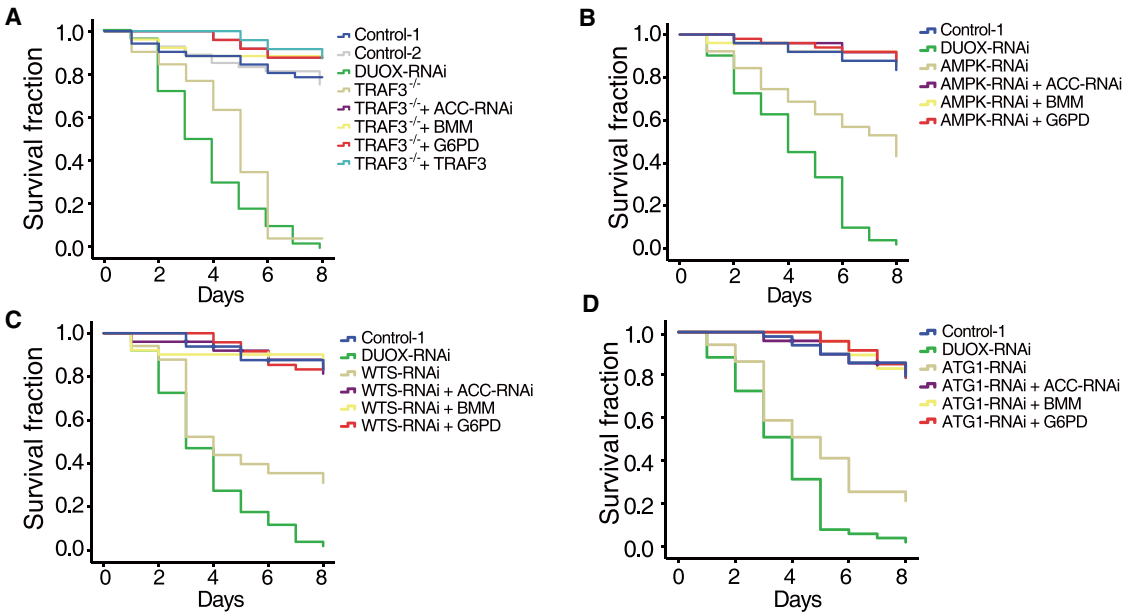

Figure 7. TRAF3-AMPK/WTS-ATG1 Pathway Is Required for Host Survival during Enteric Infection by Modulating Lipid Metabolism and NADPH Homeostasis

Host survival rate following gut infection. Survival rates of *TRAF3*$^{-/-}$ (A), *AMPK-RNAi* (B), *WTS-RNAi* (C), and *ATG1-RNAi* (D) were examined at 29°C following *Ecc15* infection. Each mutant or knockdown animal is rescued by either blocking lipogenesis (by *ACC-RNAi* overexpression), enhancing lipolysis (by *BMM* overexpression), or elevating NADPH-generating cellular glycolysis levels (by *G6PD* overexpression). *DUOX-RNAi* animal is used as a positive control. A log-rank analysis (n = ~75 animals for each genotype) showed a significant difference in survival between control flies and mutant/RNAi flies ($p < 0.001$) as well as between mutant/RNAi flies and rescued flies ($p < 0.001$). Fly genotypes used in this study are shown in Table S4.

and DUOX-based gut immunity. In this study, we further showed that WTS activation is upstream of AKT inhibition and that AKT inhibition led to S6K inhibition through TSC2 activation in DUOX-based gut immunity. It will be important to investigate whether the WTS-AKT-TSC2-S6K pathway plays a similar role in the fat body in Toll/IMD-based systemic immunity. In this regard, it is interesting to note that Toll activation can directly activate WTS in the fat body (Liu et al., 2016). Further studies are warranted to elucidate the shared aspects of immune-metabolic interactions between gut immunity and systemic immunity.

Cellular metabolism provides energy for all aspects of biological activities such as reproduction, development, and immunity. All of these biological activities require energy consumption; therefore, energy should be properly allocated to optimize the performance of animals. Operating the innate immune system is energetically expensive, which is believed to be controlled by metabolic homeostasis (Kominsky et al., 2010; Wong et al., 2016; Zmora et al., 2017). Indeed, our infection-modulated transcriptome analysis revealed that the functional category of "metabolism" is mostly affected by enteric infection (Figure 4), suggesting dynamic energy allocation pattern changes in the intestine following enteric infection. Disruption of the infection-induced metabolic reprogramming as in the case of TRAF3-AMPK/WTS-ATG1 pathway-mutant flies can lead to high susceptibility of the animal to enteric infection (Figure 7). This highlights the importance of bacterial-modulated host metabolism in gut immunity. As metabolic dysregulation is believed to be closely associated with the pathogenesis of important inflammatory diseases of mucosal epithelia such as intestine, the discovery of signaling pathways governing inflammation-induced metabolic reprogramming will greatly advance our understanding of the etiology of different mucosal diseases arising from abnormal immune-metabolic interactions. Regulating the signaling pathways governing metabolic reprogramming at the tissue or organismal levels may provide a strategy for the treatment of these diseases.

STAR★METHODS

Detailed methods are provided in the online version of this paper and include the following:

- KEY RESOURCES TABLE
- CONTACT FOR REAGENT AND RESOURCE SHARING
- EXPERIMENTAL MODEL AND SUBJECT DETAILS
  - Fly Strains and Rearing
  - Microbe Culture Conditions
  - Cell Culture Conditions
- METHOD DETAILS
  - *In Vivo* ROS Measurement
  - CRISPR-Cas9 Mediated Gene Editing
  - Immunocytochemistry
  - Western Blot Analysis
  - mRNA Sequencing and Data Analysis
  - Identification of Differentially Expressed Genes (DEGs)
  - Real-Time qPCR Analysis
  - Yeast Two Hybrid Assay
  - Gut Infection and Survival Assay

- QUANTIFICATION AND STATISTICAL ANALYSIS
  - Statistical Analysis

SUPPLEMENTAL INFORMATION

Supplemental Information includes seven figures and four tables and can be found with this article online at https://doi.org/10.1016/j.chom.2018.01.011.

ACKNOWLEDGMENTS

This work was supported by grants from the National Creative Research Initiative programs of the National Research Foundation of South Korea (2015R1A3A2033475). D.H. is supported by Institute for Basic Science (IBS-R013-A1). K.-A.L. and I.-H.J. are supported in part by Basic Science Research Program (NRF-2016R1C1B2016287 and NRF-2015R1D1A4A01019973, respectively).

AUTHOR CONTRIBUTIONS

K.-A.L., K.-C.C., D.H., J.-H.S., and W.-J.L. conceived, designed, and analyzed the experiments. K.-A.L., K.-C.C., B.K., I.-H.J., K.N., Y.E.K., M.K., and D.Y.H. performed the experiments. K.-A.L. and W.-J.L. wrote the manuscript.

Received: September 28, 2017
Revised: December 7, 2017
Accepted: January 23, 2018
Published: March 1, 2018

REFERENCES

Baker, K.D., and Thummel, C.S. (2007). Diabetic larvae and obese flies—emerging studies of metabolism in *Drosophila*. Cell Metab. *6*, 257–266.

Blow, N.S., Salomon, R.N., Garrity, K., Reveillaud, I., Kopin, A., Jackson, F.R., and Watnick, P.I. (2005). *Vibrio cholerae* infection of *Drosophila melanogaster* mimics the human disease cholera. PLoS Pathog. *1*, 92–98.

Bolstad, B.M., Irizarry, R.A., Astrand, M., and Speed, T.P. (2003). A comparison of normalization methods for high density oligonucleotide array data based on variance and bias. Bioinformatics *19*, 185–193.

Buchon, N., Osman, D., David, F.P., Fang, H.Y., Boquete, J.P., Deplancke, B., and Lemaitre, B. (2013). Morphological and molecular characterization of adult midgut compartmentalization in *Drosophila*. Cell Rep. *3*, 1725–1738.

Buchon, N., Silverman, N., and Cherry, S. (2014). Immunity in *Drosophila melanogaster*—from microbial recognition to whole-organism physiology. Nat. Rev. Immunol. *14*, 796–810.

Caron, A., Richard, D., and Laplante, M. (2015). The roles of mTOR complexes in lipid metabolism. Annu. Rev. Nutr. *35*, 321–348.

Chambers, M.C., Song, K.H., and Schneider, D.S. (2012). Listeria monocytogenes infection causes metabolic shifts in *Drosophila melanogaster*. PLoS One *7*, e50679.

Charroux, B., and Royet, J. (2012). Gut-microbiota interactions in non-mammals: what can we learn from *Drosophila*? Semin. Immunol. *24*, 17–24.

Ciechanover, A. (2005). Proteolysis: from the lysosome to ubiquitin and the proteasome. Nat. Rev. Mol. Cell Biol. *6*, 79–87.

Clark, R.I., Tan, S.W., Pean, C.B., Roostalu, U., Vivancos, V., Bronda, K., Pilátová, M., Fu, J.Q., Walker, D.W., Berdeaux, R., et al. (2013). MEF2 is an in vivo immune-metabolic switch. Cell *155*, 435–447.

Dempsey, P.W., Doyle, S.E., He, J.Q., and Cheng, G.H. (2003). The signaling adaptors and pathways activated by TNF superfamily. Cytokine Growth Factor Rev. *14*, 193–209.

Dionne, M.S., Pham, L.N., Shirasu-Hiza, M., and Schneider, D.S. (2006). Akt and foxo dysregulation contribute to infection-induced wasting in *Drosophila*. Curr. Biol. *16*, 1977–1985.

Flores, M.V., Crawford, K.C., Pullin, L.M., Hall, C.J., Crosier, K.E., and Crosier, P.S. (2010). Dual oxidase in the intestinal epithelium of zebrafish larvae has anti-bacterial properties. Biochem. Biophys. Res. Commun. *400*, 164–168.

Grasberger, H., Gao, J., Nagao-Kitamoto, H., Kitamoto, S., Zhang, M., Kamada, N., Eaton, K.A., El-Zaatari, M., Shreiner, A.B., Merchant, J.L., et al. (2015). Increased expression of DUOX2 is an epithelial response to mucosal dysbiosis required for immune homeostasis in mouse intestine. Gastroenterology *149*, 1849–1859.

Grech, A., Quinn, R., Srinivasan, D., Badoux, X., and Brink, R. (2000). Complete structural characterisation of the mammalian and *Drosophila* TRAF genes: implications for TRAF evolution and the role of RING finger splice variants. Mol. Immunol. *37*, 721–734.

Ha, E.M., Lee, K.A., Park, S.H., Kim, S.H., Nam, H.J., Lee, H.Y., Kang, D., and Lee, W.J. (2009a). Regulation of DUOX by the G alpha q-phospholipase C beta-Ca^{2+} pathway in *Drosophila* gut immunity. Dev. Cell *16*, 386–397.

Ha, E.M., Lee, K.A., Seo, Y.Y., Kim, S.H., Lim, J.H., Oh, B.H., Kim, J., and Lee, W.J. (2009b). Coordination of multiple dual oxidase-regulatory pathways in responses to commensal and infectious microbes in drosophila gut. Nat. Immunol. *10*, 949–957.

Ha, E.M., Oh, C.T., Bae, Y.S., and Lee, W.J. (2005). A direct role for dual oxidase in *Drosophila* gut immunity. Science *310*, 847–850.

Ha, H., Han, D., and Choi, Y. (2009c). TRAF-mediated TNFR-family signaling. Curr. Protoc. Immunol. *Chapter 11*, Unit11.19D.

Hacker, H., Tseng, P.H., and Karin, M. (2011). Expanding TRAF function: TRAF3 as a tri-faced immune regulator. Nat. Rev. Immunol. *11*, 457–468.

Hang, S., Purdy, A.E., Robins, W.P., Wang, Z., Mandal, M., Chang, S., Mekalanos, J.J., and Watnick, P.I. (2014). The acetate switch of an intestinal pathogen disrupts host insulin signaling and lipid metabolism. Cell Host Microbe *16*, 592–604.

Hardie, D.G. (2008). AMPK and raptor: matching cell growth to energy supply. Mol. Cell *30*, 263–265.

Hooper, L.V., Littman, D.R., and Macpherson, A.J. (2012). Interactions between the microbiota and the immune system. Science *336*, 1268–1273.

Hotamisligil, G.S. (2006). Inflammation and metabolic disorders. Nature *444*, 860–867.

Huang, D.W., Sherman, B.T., and Lempicki, R.A. (2009). Systematic and integrative analysis of large gene lists using DAVID bioinformatics resources. Nat. Protoc. *4*, 44–57.

Huang, J., and Manning, B.D. (2008). The TSC1-TSC2 complex: a molecular switchboard controlling cell growth. Biochem. J. *412*, 179–190.

Kominsky, D.J., Campbell, E.L., and Colgan, S.P. (2010). Metabolic shifts in immunity and inflammation. J. Immunol. *184*, 4062–4068.

Kondo, S., and Ueda, R. (2013). Highly improved gene targeting by germline-specific Cas9 expression in *Drosophila*. Genetics *195*, 715–721.

Kwon, Y., Song, W., Droujinine, I.A., Hu, Y.H., Asara, J.M., and Perrimon, N. (2015). Systemic organ wasting induced by localized expression of the secreted insulin/IGF antagonist ImpL2. Dev. Cell *33*, 36–46.

Laplante, M., and Sabatini, D.M. (2009). An emerging role of mTOR in lipid biosynthesis. Curr. Biol. *19*, R1046–R1052.

Laplante, M., and Sabatini, D.M. (2012). mTOR signaling in growth control and disease. Cell *149*, 274–293.

Lee, K.A., Kim, B., Bhin, J., Kim, D.H., You, H., Kim, E.K., Kim, S.H., Ryu, J.H., Hwang, D., and Lee, W.J. (2015). Bacterial uracil modulates *Drosophila* DUOX-dependent gut immunity via hedgehog-induced signaling endosomes. Cell Host Microbe *17*, 191–204.

Lee, K.A., Kim, S.H., Kim, E.K., Ha, E.M., You, H., Kim, B., Kim, M.J., Kwon, Y., Ryu, J.H., and Lee, W.J. (2013). Bacterial-derived uracil as a modulator of mucosal immunity and gut-microbe homeostasis in *Drosophila*. Cell *153*, 797–811.

Lee, W.J., and Brey, P.T. (2013). How microbiomes influence metazoan development: insights from history and drosophila modeling of gut-microbe interactions. Annu. Rev. Cell Dev. Biol. *29*, 571–592.

Lee, W.J., and Hase, K. (2014). Gut microbiota-generated metabolites in animal health and disease. Nat. Chem. Biol. *10*, 416–424.

Lemaitre, B., and Hoffmann, J. (2007). The host defense of *Drosophila melanogaster*. Annu. Rev. Immunol. *25*, 697–743.

Leto, T.L., and Geiszt, M. (2006). Role of Nox family NADPH oxidases in host defense. Antioxid. Redox Signal. *8*, 1549–1561.

Liu, B., Zheng, Y.G., Yin, F., Yu, J.Z., Silverman, N., and Pan, D.J. (2016). Toll receptor-mediated hippo signaling controls innate immunity in *Drosophila*. Cell *164*, 406–419.

Locksley, R.M., Killeen, N., and Lenardo, M.J. (2001). The TNF and TNF receptor superfamilies: integrating mammalian biology. Cell *104*, 487–501.

Ma, X., Huang, J., Yang, L., Yang, Y., Li, W., and Xue, L. (2012). NOPO modulates Egr-induced JNK-independent cell death in *Drosophila*. Cell Res. *22*, 425–431.

Manning, G., Whyte, D.B., Martinez, R., Hunter, T., and Sudarsanam, S. (2002). The protein kinase complement of the human genome. Science *298*, 1912–1934.

Martin, M. (2011). Cutadapt removes adapter sequences from high-throughput sequencing reads. ENBnet J. *17*, 10–12.

McFall-Ngai, M., Hadfield, M.G., Bosch, T.C.G., Carey, H.V., Domazet-Loso, T., Douglas, A.E., Dubilier, N., Eberl, G., Fukami, T., Gilbert, S.F., et al. (2013). Animals in a bacterial world, a new imperative for the life sciences. Proc. Natl. Acad. Sci. USA *110*, 3229–3236.

Merkle, J.A., Rickmyre, J.L., Garg, A., Loggins, E.B., Jodoin, J.N., Lee, E., Wu, L.P., and Lee, L.A. (2009). No poles encodes a predicted E3 ubiquitin ligase required for early embryonic development of *Drosophila*. Development *136*, 449–459.

Mistry, R., Kounatidis, I., and Ligoxygakis, P. (2016). Exploring interactions between pathogens and the *Drosophila* gut. Dev. Comp. Immunol. *64*, 3–10.

Rui, L. (2014). Energy metabolism in the liver. Compr. Physiol. *4*, 177–197.

Ryu, J.H., Kim, S.H., Lee, H.Y., Bai, J.Y., Nam, Y.D., Bae, J.W., Lee, D.G., Shin, S.C., Ha, E.M., and Lee, W.J. (2008). Innate immune homeostasis by the homeobox gene caudal and commensal-gut mutualism in *Drosophila*. Science *319*, 777–782.

Saxton, R.A., and Sabatini, D.M. (2017). mTOR signaling in growth, metabolism, and disease. Cell *169*, 361–371.

Schwenk, A., and Macallan, D.C. (2000). Tuberculosis, malnutrition and wasting. Curr. Opin. Clin. Nutr. Metab. Care *3*, 285–291.

Shackelford, D.B., and Shaw, R.J. (2009). The LKB1-AMPK pathway: metabolism and growth control in tumour suppression. Nat. Rev. Cancer *9*, 563–575.

Shanahan, F. (2013). The colonic microbiota in health and disease. Curr. Opin. Gastroenterol. *29*, 49–54.

Singh, R., and Cuervo, A.M. (2011). Autophagy in the cellular energetic balance. Cell Metab. *13*, 495–504.

Singh, R., Kaushik, S., Wang, Y.J., Xiang, Y.Q., Novak, I., Komatsu, M., Tanaka, K., Cuervo, A.M., and Czaja, M.J. (2009). Autophagy regulates lipid metabolism. Nature *458*, 1131–1135.

Trapnell, C., Pachter, L., and Salzberg, S.L. (2009). TopHat: discovering splice junctions with RNA-seq. Bioinformatics *25*, 1105–1111.

Trapnell, C., Williams, B.A., Pertea, G., Mortazavi, A., Kwan, G., van Baren, M.J., Salzberg, S.L., Wold, B.J., and Pachter, L. (2010). Transcript assembly and quantification by RNA-Seq reveals unannotated transcripts and isoform switching during cell differentiation. Nat. Biotechnol. *28*, 511–515.

van der Hoeven, R., Cruz, M.R., Chavez, V., and Garsin, D.A. (2015). Localization of the dual oxidase BLI-3 and characterization of its NADPH oxidase domain during infection of *Caenorhabditis elegans*. PLoS One *10*, e0124091.

Wallace, H.A., Merkle, J.A., Yu, M.C., Berg, T.G., Lee, E., Bosco, G., and Lee, L.A. (2014). TRIP/NOPO E3 ubiquitin ligase promotes ubiquitylation of DNA polymerase eta. Development *141*, 1332–1341.

Weidberg, H., Shvets, E., and Elazar, Z. (2009). Lipophagy: selective catabolism designed for lipids. Dev. Cell *16*, 628–630.

Wong, A.C.N., Vanhove, A.S., and Watnick, P.I. (2016). The interplay between intestinal bacteria and host metabolism in health and disease: lessons from *Drosophila melanogaster*. Dis. Model. Mech. *9*, 271–281.

Yao, Z.C., Wang, A.L., Li, Y.S., Cai, Z.H., Lemaitre, B., and Zhang, H.Y. (2016). The dual oxidase gene BdDuox regulates the intestinal bacterial community homeostasis of *Bactrocera dorsalis*. ISME J. *10*, 1037–1050.

Yu, F.X., and Guan, K.L. (2013). The Hippo pathway: regulators and regulations. Genes Dev. *27*, 355–371.

Zmora, N., Bashiardes, S., Levy, M., and Elinav, E. (2017). The role of the immune system in metabolic health and disease. Cell Metab. *25*, 506–521.

STAR★METHODS

KEY RESOURCES TABLE

REAGENT or RESOURCE	SOURCE	IDENTIFIER
Antibodies		
Anti-Cad99C	Lee et al., 2015	RRID: AB_2568534
Mouse monoclonal anti-V5	Invitrogen	Cat#R960-25; RRID: AB_2556564
Rabbit polyclonal anti-FLAG	Sigma-Aldrich	Cat#F7425; RRID: AB_439687
Mouse monoclonal anti-Rab7	Abcam	Cat#ab50533; RRID: AB_882241
Rabbit polyclonal anti-LAMP1	Abcam	Cat#ab30687; RRID: AB_775973
Rabbit monoclonal anti-phospho-AMPKα	Cell Signaling Technology	Cat#2535; RRID: AB_331250
Rabbit anti-LacZ	MP Biomedicals	Cat#559761; RRID: AB_2687418
Anti-β-actin	Cell Signaling Technology	Cat#3700; RRID: AB_2242334
Alexa 568 goat anti-mouse IgG	Invitrogen	Cat#A11004; RRID: AB_141371
Alexa 568 goat anti-rabbit IgG	Invitrogen	Cat#A11011; RRID: AB_143157
Alexa 488 goat anti-rabbit IgG	Invitrogen	Cat#A11008; RRID: AB_143165
Bacterial and Virus Strains		
Erwinia carotovora subsp. *carotovora* 15 (*Ecc15*)	Bruno Lemaitre Lab. École polytechnique fédérale de Lausanne	N/A
Chemicals, Peptides, and Recombinant Proteins		
HOCl-specific rhodamine-based R19S dye	Lee et al., 2013	N/A
Uridine	Sigma-Aldrich	Cat#U3750
Mifepristone	Sigma-Aldrich	Cat#M8046
MG-132	Sigma-Aldrich	Cat#M7449
3-methyladenine (3-MA)	Sigma-Aldrich	Cat#M9281
AICAR	Sigma-Aldrich	Cat#A9978
Rapamycin	Sigma-Aldrich	Cat#R0395
Bodipy 493/503	Thermo Fisher Scientific	Cat#D3922
4′,6-Diamidino-2-phenylindole dihydrochloride(DAPI)	Sigma-Aldirich	Cat#D9542
Critical Commercial Assays		
Illumina Truseq RNA Sample Prep Kit	Illumina	RS-930-1012
Illumina True-seq RNA sample prep kit v2	Illumina	RS-122-9001
SensiFAST SYBR Hi-ROX Kit	Bioline	Cat#BIO-92020
FuGENE6 Transfection Reagent	Promega	Cat#E2691
MATCHMAKER system 2 kit	Clontech	N/A
Deposited Data		
Raw and analyzed data	This paper	GEO: GSE99642
D. melanogaster reference genome (NCBI build 5.3)	NCBI Genome	https://www.ncbi.nlm.nih.gov/genome/
Experimental Models: Cell Lines		
D. melanogaster: Cell line S2	ThermoFisher	Cat#R69007
Experimental Models: Organisms/Strains		
nos-Cas9	NIG-FLY	CAS-0001
Ex-lacZ	Bloomington Drosophila stock center (BDSC)	#44248; RRID: BDSC_44248
Lsd2-YFP	Kyoto Stock Center Drosophila Genomics and Genetic Resources (DGGR)	#115181; RRID: DGGR_115181

(*Continued on next page*)

Continued

REAGENT or RESOURCE	SOURCE	IDENTIFIER
NOPO$^{-/-}$	Laura A. Lee Lab, University of Vanderbilt University School of Medicine	N/A
TRAF3$^{-/-}$	This paper	N/A
Transgene carrying TRAF3 genomic fragment	This paper	N/A
UAS-ACC	BDSC	#63224; RRID: BDSC_63224
UAS-ACC-RNAi	Vienna Drosophila Resource Center (VDRC)	#v108631
UAS-AKT-CA	Jun Hee Lee Lab, University of Michigan	N/A
UAS-AKT-RNAi	VDRC	#v103703
UAS-AMPK	BDSC	#32108; RRID: BDSC_32108
UAS-AMPK	BDSC	#32182; RRID: BDSC_32182
UAS-AMPK-RNAi	VDRC	#v1827
UAS-ATG1-RNAi	VDRC	#v16133
UAS-ATG8-RFP	Thomas P. Neufeld Lab, University of Minnesota	N/A
UAS-BEN-RNAi	VDRC	#v109638
UAS-BMM	Jiwon Shim Lab, Hanyang University	N/A
UAS-BMM-RNAi	VDRC	#v37880
UAS-Cad99C-GFP	This laboratory	N/A
UAS-DUOX-RNAi	This laboratory	N/A
UAS-FAS-RNAi	VDRC	#v108339
UAS-G6PD	William C. Orr Lab, Southern Methodist University	UAS-G6PD 4C
UAS-MEKK1-RNAi	VDRC	#v25528
UAS-NOPO-RNAi	This paper	N/A
UAS-NOPO-WT-FLAG_pMTa	This paper	N/A
UAS-RHEB	Jun Hee Lee Lab, University of Michigan	N/A
UAS-RHEB-RNAi	SHared Information of GENetic Resources (SHIGEN)	#1081R-2
UAS-S6K-CA	Scott Pletcher Lab, University of Michigan	N/A
UAS-S6K-DN	Scott Pletcher Lab, University of Michigan	N/A
UAS-SREBP	Jongkyeong Chung Lab, Seoul National University	N/A
UAS-SREBP-RNAi	Jongkyeong Chung Lab, Seoul National University	N/A
UAS-TOR-DN	Scott Pletcher Lab, University of Michigan	N/A
UAS-TRAF1-RNAi	VDRC	#v21214
UAS-TRAF2-RNAi	VDRC	#v16125
UAS-TRAF3-RNAi	This paper	N/A
UAS-TRAF3-V5_pMTa	This paper	N/A
UAS-TSC2	Scott Pletcher Lab, University of Michigan	N/A
UAS-TSC2-RNAi	VDRC	#v6313
UAS-UEV1A-RNAi	VDRC	#v107465
UAS-WTS	Ryan S. Udan Lab, Baylor College of Medicine	N/A
UAS-WTS-RNAi	VDRC	#v106174
UAS-Yorkie-RNAi	VDRC	#v104523
NP1-GAL	Bruce A. Edgar Lab, Center for Molecular Biology Heidelberg University (ZMBH) Alliance	N/A
NP1-GAL4;Tub-GAL80ts	Bruce A. Edgar Lab, Center for Molecular Biology Heidelberg University (ZMBH) Alliance	N/A

(*Continued on next page*)

Continued

REAGENT or RESOURCE	SOURCE	IDENTIFIER
HS-GAL4	BDSC	#1799; RRID: BDSC_1799
5966GS-GAL4	Heinrich Jasper Lab, Buck institute for Research on Aging	N/A
UAS-Ci-RNAi	VDRC	#v51479
UAS-Cos-RNAi	VDRC	#v108914
Daughterless–GAL4 (Da–GAL4)	Lee et al., 2013	N/A
Oligonucleotides		
RNA sequence: gRNA1 targeting TRAF3 coding region: GCAACGCATGAGTGTCAGCA	This paper	N/A
RNA sequence: gRNA2 targeting TRAF3 coding region: GCCTGCTTGAACGTTCTATC	This paper	N/A
Primers for real-time qPCR: see Table S3	This paper	N/A
Recombinant DNA		
pBFv-U6.2 vector	Kondo and Ueda, 2013	N/A
pAS2-BD-TRAF3	This paper	N/A
pACT2-AD-NOPO	This paper	N/A
pNOPO-WT-FLAG	This paper	N/A
pNOPO-I8G-FLAG	This paper	N/A
pTRAF3-V5	This paper	N/A
Software and Algorithms		
Cutadapt v.1.6	Martin, 2011	http://cutadapt.readthedocs.io/en/stable/index.html; RRID: SCR_011841
TopHat v.2.0.7	Trapnell et al., 2009	https://ccb.jhu.edu/software/tophat/index.shtml; RRID: SCR_013035
Cufflinks v.2.0.2	Trapnell et al., 2010	http://cole-trapnell-lab.github.io/cufflinks/; RRID: SCR_014597
DAVID v.6.8	Huang et al., 2009	https://david.ncifcrf.gov/home.jsp; RRID: SCR_001881
SPSS software	IBM Corporation	https://www.ibm.com/kr-ko/marketplace/spss-statistics; RRID: SCR_002865
ImageJ	US National Institutes of Health	https://imagej.nih.gov/ij/download.html; RRID: SCR_003070

CONTACT FOR REAGENT AND RESOURCE SHARING

Further information and requests for resources and reagents should be directed to and will be fulfilled by the Lead Contact, Won-Jae Lee (lwj@snu.ac.kr).

EXPERIMENTAL MODEL AND SUBJECT DETAILS

Fly Strains and Rearing

The fly lines used in this study are summarized in the Key Resources Table. A detailed fly genotypes used in this study are provide in the Table S4. All fly lines were reared at 25 °C on Bloomington Drosophila stock center's standard cornmeal medium. For the experiment using temperature-sensitive GAL4 drivers, *HS-GAL4* (containing heat shock promoter-controlled GAL4) and *NP1-GAL4^{ts}* (containing both *NP1-GAL4* and the temperature-sensitive GAL4 inhibitor under control of tubulin promoter, *tub-GAL80^{ts}*) were used. These flies were shifted to 29 °C at the adult stage for 2 days before experiments. In the case of survival experiment using flies carrying HS-GAL4, the experiment was performed at 29 °C. For the experiment using mifepristone-inducible GAL4 driver, *5966GS-GAL4*, RU486 was added to the food vial at the final concentration of 0.2 mg/ml. Adult male flies (5- to 6-day-old) were used in the survival experiments. For the in vivo ROS measurement and confocal image analyses, we mainly used adult female flies (5- to 6-day-old), unless explicitly written in the figure legends.

Microbe Culture Conditions

Ecc15 strain is obtained from Bruno Lemaitre. For experiment, 10 ml of Luria-Bertani (LB) broth was inoculated with a bacterial colony from LB plate for 12 hr at 30°C with vigorous agitation (~200 rpm). This bacterial culture was further diluted with 1 liter of fresh LB for overnight culture. The next day, culture was centrifuged at 4,000 rpm for 20 min, pellets were resuspended in 5% sucrose solution for enteric infection by oral ingestion. A 5% sucrose solution containing $\sim 10^9$ cells (for *in vivo* ROS measurement, confocal image analysis, and real-time qPCR analysis) or $\sim 10^{10}$ cells of Ecc15 (for mRNA-sequencing analysis and survival experiments) was used.

Cell Culture Conditions

Drosophila S2 cells were cultured with Schneider media containing 10% fetal bovine serum (HyClone™, GE Healthcare Life Sciences) supplemented with 100 U/ml penicillin-streptomycin, and were maintained in 26°C incubator without CO_2.

METHOD DETAILS

In Vivo ROS Measurement

To measure DUOX-dependent ROS generation *in vivo*, The R2 region of the intestine was stained with HOCl-specific rhodamine-based R19S dye as described previously (Lee et al., 2013). DUOX activity was shown as percentage of R19S-positive gut.

CRISPR-Cas9 Mediated Gene Editing

CRISPR-Cas9 mediated gene editing was performed as described previously (Kondo and Ueda, 2013). Two gRNA sequences were used to target Cas9 to the TRAF3 coding region; gRNA1: 5'-GCA ACG CAT GAG TGT CAG CA-3' and gRNA2: 5'-GCC TGC TTG AAC GTT CTA TC-3'. Two different gRNAs were cloned into pBFv-U6.2 vector. This double gRNA vector targeting TRAF3 was injected into the embryos to generate transgenic flies. Female transgenic flies carrying U6-gRNA were crossed to male transgenic flies carrying nos-Cas9 to obtain founder animals that have both the U6-gRNA and the nos-Cas9 transgenes. Individual founder animals were crossed and TRAF3 mutant animal was screened by PCR amplification of target locus.

Immunocytochemistry

Drosophila S2 cells were fixed for 5 min with 4% paraformaldehyde. The midguts were dissected in PBS and then fixed for 15 min with 4% paraformaldehyde. Samples were washed three times for 5 min with 0.1% Triton X-100 in PBS and incubated with the same solution supplemented with 5% bovine serum albumin for 20 min. The samples were incubated with anti-Cad99C antibody (1:500 dilution) (Lee et al., 2015), anti-V5 antibody (1:500 dilution; Invitrogen), anti-FLAG antibody (1:500 dilution; Sigma-Aldrich), anti-Rab7 antibody (1:500 dilution; Abcam), anti-LAMP1 antibody (1:500 dilution; Abcam), anti-phospho-AMPK antibody (1:100 dilution; Cell Signaling), or anti-LacZ antibody (1:1,000 dilution; MP Biomedicals) for 16 hr at 4°C. The samples were then washed five times for 5 min in PBS with 0.1% Triton X-100. For the secondary antibodies, Alexa Fluor 568 goat anti-mouse IgG, Alexa Fluor 568 goat anti-rabbit IgG, or Alexa Fluor 488 goat anti-rabbit (Invitrogen) was used. Following three washes in PBS with 0.1% Triton X-100 for 5 min each, the samples were mounted in mounting buffer (Vectorshield, Vector Laboratories Inc.). In all cases, upper region of the copper cells, equivalent to R2b and R2c subdomains (Buchon et al., 2013), was analyzed by confocal microscopy LSM 700 (Carl Zeiss). Nuclear staining was performed with DAPI.

Western Blot Analysis

Wild type NOPO (NOPO-WT) or NOPO-I8G were co-transfected with TRAF3 into S2 cells by using FuGENE 6 reagent (Promega) according to manufacturer's instruction. Transfection experiments were performed in the presence of proteasome inhibitor (2 μM of MG132 for 12 hr) or lysosome inhibitor [10 mM of 3-methyladenine (3-MA) for 12 hr]. TRAF3 and NOPO were V5 and FLAG epitope-tagged, respectively. Western blot analysis was performed using anti-V5 (dilution 1:5000) and anti-FLAG antibody (dilution 1:10000). Anti-β-actin antibody (dilution 1:10000) was used as loading controls.

mRNA Sequencing and Data Analysis

Adult flies were orally administered a 5% sucrose solution containing $\sim 10^{10}$ cells of *Ecc15* for mRNA sequencing analysis. Midguts ($n = 80$ for each time point) were dissected (at 2, 4 and 16 hr post-infection) and total RNAs were prepared. Control vehicle treatment (i.e. oral ingestion of sucrose without bacteria) was used as a control. Poly(A) mRNA isolation from total RNAs (5 μg) and fragmentation were performed using the Illumina Truseq RNA Sample Prep Kit with poly-T oligo-attached magnetic beads. Libraries were prepared for multiplex sequencing using Illumina True-seq RNA sample prep kit v2, according to the manufacturer's protocol. The adaptor ligated libraries were sequenced using an Illumina Hi-Seq 2000 (DNA Link, Korea). From the resulting read sequences for each sample, adapter sequences (TruSeq universal and indexed adapters) were removed using the cutadapt software (ver. 1.6) (Martin, 2011). The resulting reads were then aligned to the *Drosophila melanogaster* reference genome (NCBI build 5.3) using TopHat aligner (Trapnell et al., 2009) (ver. 2.0.7) with the default options. After the alignment, we estimated fragments per kilobase of transcript per million fragments mapped (FPKM) using Cufflinks (Trapnell et al., 2010) (ver. 2.0.2). The raw and normalized data of mRNA-sequencing were deposited at the Gene Expression Omnibus database (GSE99642).

Identification of Differentially Expressed Genes (DEGs)

We first identified 'expressed' genes as the ones with FPKM > 1 in at least one of the six samples (one sample per condition). For these expressed genes, the FPKM values were converted to $\log_2$-FPKM after adding one to the FPKM values. The $\log_2$-FPKM for the samples were then normalized using the quantile normalization method (Bolstad et al., 2003). We then identified DEGs as the ones with absolute $\log_2$-fold-changes >0.58 (1.5-fold) for the comparisons of infected samples versus control samples in same time points. To identify cellular processes represented by the DEGs, we performed the enrichment analysis of gene ontology biological processes (GOBPs) for the genes using DAVID software (Huang et al., 2009) and selected the GOBPs with p-value < 0.05 as the processes enriched by the DEGs. Moreover, for network analysis, the DEGs involved in fatty acid biosynthetic process were mapped into 'fatty acid biosynthesis' and 'glycerolipid metabolism' pathways in Kyoto Encyclopedia of Genes and Genomes (KEGG) pathway database, and metabolic reactions catalyzed by the DEGs were compiled into a metabolic network model for fatty acid synthesis.

Real-Time qPCR Analysis

Fluorescence real-time PCR was performed to quantify gene expression, using the double-stranded DNA dye, SYBR Green (Bioline). SYBR Green analysis was performed using an ABI PRISM 7700 system (PE Applied Biosystems) according to the manufacturer's instructions. Primer pairs were used to detect different target gene transcripts (Table S3). All samples were analyzed in triplicate, and the normalized data were then used to quantify the relative levels of a given mRNA according to the cycling threshold analysis. Target gene expression is presented as relative expression level.

Yeast Two Hybrid Assay

The recombinant plasmid containing GAL4 DNA-binding domain (BD) fused in-frame to the full-length TRAF3 (pAS2-BD-TRAF3) and the recombinant plasmid containing GAL4 activation domain (AD) fused in-frame to the full-length NOPO (pACT2-AD-NOPO) were constructed as suggested by the manufacturer's instruction (Clontech). The control plasmids containing GAL4 AD fused to SV40 large T antigen (pACT2-AD-SV40) or GAL4 BD fused to human lamin C (pAS2-BD-laminC) were provided by MATCHMAKER system 2 kit (Clontech). Yeast Y190 cells were co-transformed with pAS2-BD-TRAF3 and pACT2-AD-NOPO, and transfomants were cultured on synthetic drop-out medium in the absence of histidine to visualize the interaction between NOPO and TRAF3.

Gut Infection and Survival Assay

Adult male flies (5- to 6-day-old) were used in this experiment. Oral infection with *E. carotovora* was performed exactly as describe previously (Lee et al., 2013).

QUANTIFICATION AND STATISTICAL ANALYSIS

Statistical Analysis

SPSS software (Chicago, IL, USA) was used for all analyses. Comparisons of two samples and multiple samples were made by Student's t test and one-way analysis of variance (ANOVA), respectively. The log rank test of the Kaplan-Meier was used for the statistical analysis of fly survival experiments. p values of less than 0.05 were considered statistically significant. For each figure, the number of experimental replicates or samples as well as other information relevant for the statistical analysis are included in the accompanying legend.